

This discussion paper is/has been under review for the journal Atmospheric Chemistry and Physics (ACP). Please refer to the corresponding final paper in ACP if available.

Ozone production and transport over the Amazon Basin during the dry-to-wet and wet-to-dry transition seasons

M. M. Bela^{1,*}, K. M. Longo², S. R. Freitas², D. S. Moreira², V. Beck³, S. C. Wofsy⁴, C. Gerbig³, K. Wiedemann⁴, M. O. Andreae⁵, and P. Artaxo⁶

¹Center for Earth System Science (CCST), National Institute for Space Research (INPE), São José dos Campos, Brazil

²Center for Weather Forecast and Climate Studies, National Institute for Space Research (INPE), Cachoeira Paulista, Brazil

³Max Planck Institute for Biogeochemistry, Jena, Germany

⁴Division of Engineering and Applied Science/Department of Earth and Planetary Science, Harvard University, Cambridge, MA, USA

⁵Biogeochemistry Department, Max Planck Institute for Chemistry, Mainz, Germany

⁶Institute of Physics, University of São Paulo, São Paulo, Brazil

* now at: Laboratory for Atmospheric and Space Physics, University of Colorado, Boulder, USA

14005

Received: 21 March 2014 – Accepted: 1 May 2014 – Published: 2 June 2014

Correspondence to: M. M. Bela (megan.bela@colorado.edu)

Published by Copernicus Publications on behalf of the European Geosciences Union.

14006

Abstract

The Regional Carbon Balance in Amazonia (BARCA) campaign provided the first Amazon Basin-wide aircraft measurements of O_3 during both the dry-to-wet (November and December 2008) and wet-to-dry (May 2009) transition seasons. Extremely low background values (< 20 ppb) were observed to the west and north of Manaus in both seasons and in all regions during the wet-to-dry transition. On the other hand, elevated O_3 levels (40–60 ppb) were seen during the dry-to-wet transition to the east and south of Manaus, where biomass burning emissions of O_3 precursors were present. Chemistry simulations with the CCATT-BRAMS and WRF-Chem models are within the error bars of the observed O_3 profiles in the boundary layer (0–3 km a.s.l.) in polluted conditions. However, the models overestimate O_3 in the boundary layer in clean conditions, despite lacking the predominant NO source from soil. In addition, O_3 simulated by the models was either within the error bars or lower than BARCA observations in mid-levels (3–5 km a.s.l.), indicating that the models do not represent the free troposphere – boundary layer gradient in O_3 . Total tropospheric O_3 retrieved from OMI/MLS was higher than that simulated by the models, suggesting that the satellite observations are dominated by the middle troposphere and long-range processes and are not a good indication of O_3 conditions in the PBL. Additional simulations with WRF-Chem showed that the model O_3 production is very sensitive to both the O_3 deposition velocities, which were about one half of observed values, and the NO_x emissions. These results have implications for the monitoring and prediction of increases in O_3 production in the Amazon Basin as the regional population grows.

1 Introduction

In the Amazon Basin, trace gases from biomass-burning, urban, and biogenic emissions are important sources of ozone precursors, which are efficiently transported by intense convective activity to the upper troposphere, where they can be dispersed over

14007

long distances by regional and global circulations. Additionally, convective overshooting may inject heat, moisture and trace gases into the tropical tropopause layer, impacting stratospheric ozone and other aspects of global climate (Fueglistaler et al., 2009). In the dry-to-wet transition season, regional smoke and haze plumes from biomass burning are observed (Longo et al., 2009). On the other hand, in the wet-to-dry transition season, biogenic emission of VOCs, particularly from the Amazon rainforest, may maintain the atmospheric oxidative capacity for generating ozone and other photochemical pollutants (Lelieveld et al., 2008). Inhalation of elevated levels of ozone can irritate the lungs; aggravate asthma and cause emphysema, bronchitis, and premature death (Schwela, 2000). High ozone concentrations can also inhibit photosynthesis in plants and damage leaf tissue, harming wild ecosystems and reducing crop productivity (Reich and Amundson, 1985). In the upper troposphere, O_3 acts as a greenhouse gas, increasing surface radiative forcing (IPCC, 2001). The Amazon Basin continues to rapidly urbanize, and urban emissions of O_3 precursors are also expected to grow (Gallardo et al., 2010). An improved understanding/quantification of O_3 temporal and spatial variability in the tropical rainforest environment is important for projecting future impacts of land use and climate change in the Amazon Basin and other tropical rainforest regions worldwide on their expanding human populations and significant biodiversity.

Motivated by the impact of O_3 in the Amazon Basin on human and ecosystem health and global climate, we collected aircraft observations of O_3 during BARCA and conducted regional chemistry simulations in order to answer the following scientific questions: how does O_3 vary spatially and seasonally over the Amazon Basin? What are the sources and sink of O_3 in this region? How well can state-of-the-art regional chemistry models reproduce O_3 distributions over the Amazon Basin?

Previous analyses of satellite ozone data have noted early-year O_3 maximums in the tropical Southern Hemisphere primarily associated with cross-Atlantic transport of biomass burning emissions from Africa (Thompson et al., 1996), Northern Hemisphere fires and lightning NO_x (Edwards et al., 2003). In the Amazon region, ground-based

14008

and aircraft campaigns (e.g., Kirchhoff et al., 1990; Browell et al., 1996; Kaufman et al., 1998; Longo et al., 1999; Cordova et al., 2003; Andreae et al., 2001, 2002; Rummel et al., 2007; Kuhn et al., 2010; Martin et al., 2010; Toon et al., 2010) have observed both background O₃ levels of 10–20 ppb and elevated levels of 60–80 ppb due to production from regional fire emissions and recirculated urban pollution from SE Brazil, as well as evidence of deep convective transport of boundary layer air to the middle and upper troposphere.

In-situ data on cloud properties and chemical species, as well as observations of land use changes, boundary layer dynamics and larger-scale cloud-aerosol interactions, are scant in this region. Therefore, models are essential tools for monitoring and predicting atmospheric chemistry composition, weather, and climate at local, regional, and global scales. Uncertainties in the model representations of parameterized convection, turbulence, land surface and other subgrid scale processes lead to significant errors in simulated transport and chemical transformation of the atmospheric composition (Beck et al., 2013). The Regional Carbon Balance in Amazonia (BARCA) Large-Scale Biosphere-Atmosphere (LBA) experiment was an aircraft campaign based in Manaus and conducted during the dry-to-wet (November and December 2008) and wet-to-dry (May 2009) transition seasons. BARCA was the first flight campaign to sample ozone and other trace gases on a regional scale in both transition seasons. It offers a unique opportunity, together with satellite observations and modeling studies, to understand the regional ozone distribution in the Amazon under different meteorological and emissions regimes. It is interesting to compare BARCA data to observations from the NASA Amazon Boundary Layer Experiments ABLE campaigns (ABLE-2A and -2B), which took place during the dry season of 1985 and wet-to-dry transition of 1987. Andreae et al. (2012) showed that CO mixing ratios were about 10 ppb higher during ABLE-2B than in BARCA B everywhere except the southern region, reflecting the global trend towards decreasing CO emissions since the 1980s, particularly in the Northern Hemisphere. The CO comparison also showed a similar enhancement of 10–20 ppb in the lowest 1 km above the surface, attributed to diffuse biogenic sources, and also indicated

14009

that the much higher enhancements during the dry season in BARCA A must be due to anthropogenic or biomass burning inputs. The O₃ comparison is expected to yield information in long-term trends in O₃ production in the Amazon Basin, as well as the relative importance of biogenic, urban and fire sources.

The structure of this paper is as follows. In Sect. 1.1, the measurements taken during the BARCA aircraft campaign are described, followed by the meteorological conditions and emissions regimes during the two phases of the campaign in Sect. 1.2. Section 1.3 reviews previous observational and remote sensing studies of O₃ distributions and seasonality in the Amazon. Section 2 describes the aircraft, ground-based, and remote sensing observations used in the analysis, as well as the setup of the CCATT-BRAMS and WRF-Chem simulations. In Sect. 3, the results of the analysis of meteorological and O₃ observations and simulations are presented, with final discussions and conclusions in Sect. 4.

1.1 BARCA aircraft campaigns

The BARCA flights were conducted with the EMB 110 Bandeirante aircraft of the Brazilian National Institute for Space Research (INPE). The flights consisted of quasi-Lagrangian measurements of carbon dioxide (CO₂), carbon monoxide (CO), methane (CH₄), ozone (O₃), and aerosols, and were designed to constrain basin-wide fluxes and understand distributions and sources of these species. The EMB 110 Bandeirante INPE aircraft had a ceiling of 4500 m, and flights usually consisted of ascending and descending vertical profiles separated by short (5–30 min) horizontal legs. In-situ measurements were made of CO₂, CH₄, CO, O₃, aerosol number concentration and optical properties. Flask samples were collected to determine CO₂, CH₄, sulfur hexafluoride (SF₆), CO, nitrous oxide (N₂O), hydrogen, and the oxygen-nitrogen ratio (O₂/N₂). A detailed description of the aircraft measurements can be found in Andreae et al. (2012). Figure 1 shows a map of the flight tracks from BARCA A and B. Both experiment periods included flights to the north, south and east of Manaus, as well as local flights near Manaus. Only BARCA A included flights to the west of Manaus, because intense

14010

convective activity in that region during BARCA B precluded flying. During BARCA B, fire activity was low throughout the Amazon region due to heavy precipitation, while during BARCA A, intense fire activity occurred on the northern coast of Brazil and scattered fires were present throughout the southeastern Amazon.

5 1.2 Transition season meteorology and emissions

Andreae et al. (2012) summarized the BARCA campaign, meteorological background, carbon monoxide and aerosol observations and CO results from several regional transport and chemistry models. These included the CCATT-BRAMS and WRF-Chem simulations analyzed in greater detail in this paper. Meteorological analysis showed that during BARCA A, when the Inter-Tropical Convergence Zone (ITCZ) was to the north of the Amazon Basin, inflow to the Amazon was primarily from the Southern Hemisphere. During BARCA B, the ITCZ extended to 20° S and air at low levels was of Northern Hemisphere origin, including some smoke from west African fires. On the other hand, the mid tropospheric air was of mixed origin.

15 The highest CO levels were observed on the flights on 25–27 November in the southeastern Amazon, influenced by regional biomass burning, as maximum values were observed from 1–3 km. These are typical of injection heights of smoke plumes from savanna fires (Freitas et al., 2007). The excess CO from biomass burning was between about 30 and 200 ppb, increasing from north to south across the Basin. The mean contribution from biomass burning to total CO during BARCA A was about 31 %, with a contribution from background (110 ppb) of about 61 %. Biomass burning influence was indicated by CO mixing ratios up to 300 ppb, Condensation Nuclei (CN) approaching 10 000 cm⁻³ and a low CN to CO ratio ($\Delta\text{CN}/\Delta\text{CO}$) indicating aged smoke. This influence was highest in the southern Amazon from 1–3 km. Manaus back trajectories at 500 and 4000 m came from eastern Amazon fires rather than the intense African fires occurring at the same time. During BARCA B, little biomass burning influence was observed. CN counts were 300–500 cm⁻³ and a CO enhancement of ~ 10 ppb above the mixing ratios in air entering the Basin from the Atlantic was seen. Small boundary

14011

layer enhancements were attributed to a source from the oxidation of biogenic VOCs (Andreae et al., 2012).

Andreae et al. (2012) also showed simulated vertical CO profiles from CCATT-BRAMS and WRF-Chem simulations, as well as the Stochastic Time Inverted Lagrangian Transport (STILT) model with two different meteorological field inputs and the WRF Greenhouse Gas Module (WRF-GHG). The simulated CO profiles matched mean observed values, but were overly vertical (too low near the surface and too high above 3 km). This suggested that the models had too much convective transport or vertical mixing from the PBL schemes. However, the probability densities were consistent with observations in the boundary layer, indicating that horizontal dispersion was reasonable. Beck et al. (2013) evaluated different CH₄ wetland emissions schemes and maps using WRF-GHG. They found the best agreement with BARCA CH₄ data for days where convective transport, as evaluated by comparison of upstream TRMM and WRF precipitation amounts, was well represented in the model. This indicates that proper representation of convective transport in models is essential for prediction of vertical distributions of pollutants in the Amazon Basin.

1.3 Previous studies of O₃ in the Amazon

Analyses of satellite, aircraft and ground-based observations of O₃ over Amazônia since the 1980s have demonstrated the influence of long-range transport of African biomass burning and Northern Hemisphere inputs, local fire sources, NO soil and biogenic VOC emissions, and convective transport on spatial and seasonal variability in O₃. In particular, data from the ABLE-2B aircraft and ground campaign during the 1987 wet-to-dry transition season and the BARCA observations offer the opportunity to compare the regional O₃ distribution across decades.

25 Several studies of satellite data have reported a seasonal O₃ maximum in the tropical Southern Hemisphere, largely associated with long-range transport of African fire emissions or lightning NO_x sources. Fishman and Larsen (1987) combined data from 1979–1980 from the Total Ozone Mapping Spectrometer (TOMS) and the Stratospheric

14012

Aerosol and Gas Experiment (SAGE) instruments to construct a climatology of tropospheric O_3 from $15^\circ N$ to $15^\circ S$. They attributed the most elevated O_3 from $60^\circ W$ to $60^\circ E$ to biomass burning sources. Thompson et al. (1996) integrated TOMS satellite O_3 data with observations from the Transport and Atmospheric Chemistry near the Equator-Atlantic (TRACE-A) and the southern African Fire-Atmosphere Research Initiative (SAFARI) 1992 experiments. They showed a seasonal maximum in tropospheric O_3 in the south Atlantic, with the highest values (> 90 ppb) between 0 – $25^\circ S$. Back and forward trajectories attributed this elevated O_3 to transport of O_3 from fires in southern Africa by mid-level easterlies or recirculations, with little South American contribution. In Brazil, O_3 was seen to be lofted by deep convective transport, and then transported by high-level westerlies. However, from 0 – $10^\circ S$ most of the O_3 was from Africa, since there was a delay of 1–2 months from peak African biomass burning to the O_3 maximum at the coastal site of Natal. O_3 production from the surface to 4 km was estimated to be 15 ppb O_3 per day, with a lower but nonzero rate in the upper troposphere. Using remote sensing observations of fire and lightning flash counts and NO_2 , Edwards et al. (2003) identified an early-year tropical Atlantic tropospheric O_3 maximum in January 2001. The maximum contained two peaks, the first in the lower troposphere from Northern Hemisphere fires and the second in the southern tropical Atlantic mid-troposphere from lightning NO_x .

For the Amazon region, observations of O_3 and other trace gases were made in several aircraft and ground-based campaigns. These observations identified background (absent of urban and fire influence) O_3 values of around 20 ppb originating from soil NO emissions, decreasing to very low values (~ 5 ppb) at night due to O_3 deposition to the forest. However, nighttime values can increase due to convective downdrafts, and free troposphere enhancements from biomass burning sources are seen.

The earliest O_3 measurements over the Amazon Basin were made during aircraft campaigns in the dry seasons 1979 and 1980 (Crutzen et al., 1985). Mixing ratios of 20–30 ppb and 40–50 ppb were observed in the boundary layer and the free troposphere, respectively, and elevated O_3 was attributed to photochemical reactions and

14013

biomass burning. During the dry season (July–August 1985), the Amazon Boundary Layer Experiment (ABLE-2A) integrated aircraft, ground-based and satellite observations to study the processes affecting the chemical composition in mixed layer over Amazonia (Harriss et al., 1988). Jacob and Wofsy (1988) used a photochemical model of the Amazonian boundary layer to study the diurnal cycle of isoprene, NO_y and O_3 during ABLE-2A. They found that photochemical production spurred by NO emissions from soils increased daytime O_3 to about 20 ppb. However, at night, dry deposition to the forest caused O_3 to drop below 5 ppb. Model results were consistent with the NO values of 25–60 ppt observed in the lower boundary layer over central Amazonia (Torres and Buchan, 1988). Isoprene emissions were found to have little effect on O_3 levels, as the oxidation of CO would produce sufficient HO_x to generate 20 ppb of O_3 . However, O_3 production in the model was highly sensitive to NO_x emissions, and downward transport from the free troposphere became the dominant source of O_3 in the PBL when NO emissions were decreased below the average value of $44 \pm 14 \mu g N m^{-2} h^{-1}$ NO measured by Kaplan et al. (1988). Lidar observations during ABLE-2A showed highly variable O_3 levels, with some small regions with up to 30–40 ppb, attributed to variable NO flux from the canopy (Browell et al., 1988). ABLE-2B was conducted during the wet-to-dry transition season (April–May 1987) (Harriss et al., 1990). Periodic inputs from the Northern Hemisphere were found to be a pollution source over Amazonia, and dry deposition in the region provides a significant sink in the global O_3 budget.

Aircraft measurements from TRACE-A over the south Atlantic in the 1992 dry season attributed high O_3 (> 100 ppb) in the upper troposphere to photochemical production from convectively lofted Brazilian biomass burning emissions. Elevated O_3 (> 75 ppb) originated in lower altitude (< 6 km) plumes from African fires (Browell et al., 1996). During the Smoke, Clouds, and Radiation-Brazil (SCAR-B) campaign (Kaufman et al., 1998), ozone soundings were launched at Cuiabá from 16 August–10 September 1995. Elevated ozone was attributed to both local biomass burning pollution and recirculation of urban emissions from SE Brazil. Aerosol backscatter coefficient measurements

14014

aboard the ER-2 aircraft during two flights between Cuiabá and Vilhena confirmed the co-occurrence of layers of elevated O₃ with smoke (Longo et al., 1999).

As part of ABLE-2, near-continuous O₃ surface measurements (1.5 m above the surface) showed daytime maximum of 5.7 and 3.7 ppb in a clearing and forest, respectively, and measurements in a tower in a clearing showed an increasing gradient of O₃ with height, up to 6.9 ppb at 15 m above the surface (Kirchhoff et al., 1990). Furthermore, 20 ozonesondes launched in the clearing showed typical mixing ratios of 40 ppb from 500–300 hPa, with values about 10 ppb lower in the wet than dry season.

Observations of O₃, NO_x and CO at a pasture site in the state of Rondônia and forest sites in the states of Pará and Amazonas showed elevated (3×) O₃ and NO₂ levels in the dry-to-wet transition season at the pasture site due to the influence of biomass burning. This was shown by correlations with black carbon and aerosol number concentrations at the surface. On the other hand, NO levels were much lower in the dry-to-wet transition season due to the conversion of NO₂ to NO favored by elevated levels of VOCs, O₃, and radicals, and by higher temperatures. In addition, nighttime ozone was increased in the wet season by transport of ozone-rich cold air from the mid- and upper-troposphere by convective downdrafts, as shown by an anti-correlation of O₃ with equivalent potential temperature (Cordova et al., 2003).

During the LBA-CLAIRE-98 experiment (Andreae et al., 2001) in March 1998, elevated levels of trace gases and biomass burning aerosol were observed at high altitudes (> 9 km) during a flight off the coast of Suriname. Model simulations of CO transport later confirmed the measurements to be the outflow of a deep convective system which had transported biomass burning emissions originating from the northern Amazon (Freitas et al., 2000; Andreae et al., 2001; Gevaerd et al., 2006). During the same experiment, trace gases and CCN spectra were also measured continuously at a ground station in Balbina, near Manaus (Zhou et al., 2002). During the experiment, air masses with origin over undisturbed rainforest and little anthropogenic influence, were sampled at Balbina, yielding O₃ values always less than 20 ppb. Photochemical production of O₃ of up to 15 ppb h⁻¹ was detected via aircraft transects in the Manaus

14015

urban plumes (Kuhn et al., 2010). Most of the VOC reactivity was provided by isoprene emissions from the surrounding rainforest, and NO_x emissions suppressed O₃ production close to urban sources, but stimulated it downwind.

Observations at a pasture site in Rondônia in January–February 1999 during the LBA Wet Season Atmospheric Mesoscale Campaign (WETAMC) showed that downward convective transport events increased nighttime surface O₃ up to 30 ppb, compared to a background of 3–5 ppb (Betts et al., 2002). During the LBA-EUSTACH experiments, CCN and trace gases (including O₃, NO_x and VOCs) were measured at forest and pasture sites in Rondônia in the wet-to-dry (27 April–29 May 1999) and dry-to-wet (12 September–27 October 1999) seasons (Andreae et al., 2002; Rummel et al., 2007). The observations showed VOC (isoprene, formaldehyde, acetaldehyde, acetic and formic acid) concentrations 4–5 times higher in the dry than wet-to-dry transition season. The VOC enhancement was a result of both enhanced biogenic emissions and photochemical decomposition due to increased solar radiation. In addition, VOC and O₃ concentrations peaked in the afternoon (around 15:00 LT) in both seasons and at both sites. Peak O₃ rose from ca. 15 to almost 60 ppb from the wet to dry-to-wet transition season. During the Amazonian Aerosol Characterization Experiment (AMAZE-08), O₃ was measured at the TT34 tower site from 14 February–14 March 2008 (Martin et al., 2010), with observed values of 1–20 ppb (Ebbon et al., 2011). The Tropical Composition, Clouds and Climate Coupling (TC4) experiment, based in Costa Rica in July and August of 2007, involved coordinated flights with the NASA ER-2, WB-57 and DC-8 aircraft to study convective processes in the ITCZ region (Toon et al., 2010). Using low ozone as an indicator of convective transport of boundary layer air, a maximum convective outflow height of 10–11 km was estimated (Avery et al., 2010). A flight in the boundary layer over the Columbian Amazon on 8 August 2007 measured O₃ of 10–20 ppb (R. Jiménez Pizarro, personal communication, 2012).

Thus, satellite observations enable the attribution of tropical O₃ maxima to biomass burning and lightning NO_x sources, while ground-based measurements allow the identification of key surface processes in the Amazon Basin affecting O₃ amounts. These

14016

processes include O₃ production from soil NO_x emissions and removal via dry deposition to the forest canopy. Aircraft campaigns complete the suite of observations, allowing the examination of convective lofting of surface emissions, with biomass burning emissions of particular importance on the regional scale.

5 2 Data and methods

2.1 BARCA aircraft measurements

During the BARCA campaign, in-situ measurements of O₃ were conducted aboard the EMB 110 Bandeirante INPE aircraft using a dual-cell, UV Photometric analyzer (Ozone Analyzer, Model 49i, Thermo Fisher Scientific, United States). During BARCA A, 1 min averages of the original 1 s data were taken. On the other hand, during BARCA B 1 s data were stored, and the detection limit for both campaigns was 1 ppb. The intake for O₃ was forward-facing, located 185 mm from the fuselage on the lower fuselage in front of the propellers to minimize effects of turbulence. The inlet lines consisted of stainless steel tubes with a bend radius of 100 mm and an inner diameter of 11.5 mm. The sample air was not heated or dried before measurement, so reported values are molar mixing ratios, nmol mol⁻¹, abbreviated “ppb”, with respect to ambient humid air (Andreae et al., 2012).

2.2 Satellite and ground-based O₃ and meteorological data

In addition to the in-situ O₃ data, the model results were compared with OMI/MLS monthly mean tropospheric ozone mixing ratios and total column ozone (http://acd-ext.gsfc.nasa.gov/Data_services/cloud_slice/#pub) (Ziemke et al., 2006). Tropospheric values were estimated by subtracting the stratospheric contribution from total column measurements. A cloud-slicing method was used to detect O₃ inside optically thick clouds. This method was able to detect elevated O₃ levels of around 50 ppb in the upper parts of convective clouds over South America and Africa, comparable to background

14017

cloud-free levels in the tropics (Ziemke et al., 2009). The model total tropospheric O₃ column and mean tropospheric O₃ mixing ratio were calculated by summing O₃ mixing ratios, weighted by the model level air density, from the first model level to the level below the tropopause. The tropopause level was determined by the World Meteorological Organization (WMO) definition of a temperature lapse rate less than 2 K km⁻¹ (Logan, 1999).

The models were also compared with soundings measuring O₃, temperature, and relative humidity conducted at sites in Paramaribo, Surinam (5.8° N, 55.2° W) and Natal, Brazil (5.4° S, 5.4° W) during the BARCA periods as part of the Southern Hemisphere ADDitional OZonesondes (SHADOZ) network (<http://croc.gsfc.nasa.gov/shadoz/>) (Thompson et al., 2003a, b, 2007).

Monthly mean precipitation over the Amazon region was obtained from the 3B43 Tropical Rainfall Monitoring Mission (TRMM) and Other Data Precipitation Product at a spatial resolution of 0.25° × 0.25° (obtained from <http://trmm.gsfc.nasa.gov/>) (Kummerow et al., 1998; Kawanishi et al., 2000). TRMM 3B43 is derived from retrievals of 3 hourly precipitation amount from the Precipitation Radar (PR), TRMM Microwave Imager (TMI), and Visible and Infrared Scanner (VIRS) aboard the TRMM satellite, merged with rain gauge data from Climate Anomaly Monitoring System (CAMS) and the Global Precipitation Climatology Project (GPCP). Satellite estimates of precipitation are used for model evaluation due to their more complete spatial and temporal coverage compared to rain gauge data. Buarque et al. (2011) found that mean annual rainfall from Brazilian rain gauge and TRMM 3B42 3 hourly data at 488 sites in the Amazon Basin for the years 2003–2005 agreed within 5%. Other characteristics of the rainfall distribution, such as the number of days with rainfall, differed more substantially.

Surface downward shortwave radiation (Level 1.5) observed with a Kipp and Zonen CM-21 pyranometer (305–2800 nm) were obtained from the Solar Radiation Network (SolRad-Net) site at Manaus (2.56° S, 60.04° W, 93 m a.s.l.) (http://aeronet.gsfc.nasa.gov/cgi-bin/bamgomas_interactive).

Mean daily cycles of fluxes of sensible and latent heat and radiation were obtained from flux tower measurements for the wet (February–March 1999, January–March 2000) and dry (July–September 1999–2000) seasons at forest (Rebio Jarú, 10.08° S, 61.93° W, 145 m a.s.l.) and pasture (Fazenda Nossa Senhora, 10.75° S, 62.37° W, 293 m a.s.l.) tower sites (von Randow et al., 2004).

Surface meteorological station data was obtained for the BARCA region for October–November 2008 and April–May 2009 from 52 SYNOP (INMET) and 26 METAR (airport) stations. Meteorological soundings from the Manaus airport (3.15° S, 59.98° W) were conducted at 00Z (12 in October–November 2008, 60 in April–May 2009) and 12Z (49 in October–November 2008, 60 in April–May 2009). During BARCA A, 13 additional soundings were conducted at 18Z 18 from 18 November–1 December 2008.

2.3 Model description and simulation setup

Simulations of BARCA A and B were conducted with the Chemistry Coupled Aerosol-Tracer Transport model to the Brazilian developments on the Regional Atmospheric Modeling System (CCATT-BRAMS; Longo et al., 2013; Freitas et al., 2009) and Weather Research and Forecasting with Chemistry (WRF-Chem; Grell et al., 2005) Version 3.4.1 coupled chemistry and meteorology models. The model physics and chemistry options that were used are listed in Table 1. Both models used a two-way nested grid configuration, with a 140 km grid covering Africa and South America (southwest corner: 60° S, 100° W, northeast corner: 20° N, 50° W), to encompass the cross-Atlantic transport of biomass burning emissions from Africa, and a 35 km resolution grid covering most of south America (southwest corner: 35° S, 85° W, northeast corner: 15° N, 30° W), as depicted in Fig. 3.

The simulations were initialized on 1 October 2008 00:00 UTC and 1 April 2009 00:00 UTC for BARCA A and B, respectively. Boundary conditions and analysis nudging on the outer domain were given by the NCEP GFS analysis (<http://rda.ucar.edu/datasets/ds083.2/>) with a 6 hourly time resolution and 1° × 1° spatial resolution. Chemistry initial and boundary conditions were provided by 6 hourly analyses from the

14019

Model of Atmospheric Chemistry at Large Scale (Modélisation de la Chimie Atmosphérique Grande Echelle, MOCAGE) global model (Peuch et al., 1999) with a T42 (~ 2.8°) spatial resolution. Sea surface temperature was provided by the NOAA Optimum Interpolation (OI) Sea Surface Temperature (SST) V2 (available at <http://www.esrl.noaa.gov/psd/data/gridded/data.noaa.oisst.v2.html>) with 1° × 1° spatial resolution. Soil moisture was initialized with the TRMM-based soil moisture operational product (GPNR) developed by Gevaerd and Freitas (2006).

The PBL parameterization in CCATT-BRAMS is based on Mellor and Yamada (1982), while in WRF-Chem the Mellor-Yamada-Janjic (MYJ; Janjic, 1994) scheme was used. In CCATT-BRAMS, shallow and deep convection are parameterized based on the mass-flux approach of Grell and Dévényi (2002). CCATT-BRAMS also uses the Turbulent Kinetic Energy (TKE) from the Planetary Boundary Layer (PBL) scheme to determine if convection will be triggered within a grid cell. In WRF-Chem the Grell 3-D (G3) scheme was used, which includes shallow convection and subsidence spreading of convective outflow into neighboring grid cells. The Noah land surface model (Koren et al., 1999) was used in WRF-Chem and the Land Ecosystem–Atmosphere Feedback model v.2 (LEAF-2; Walko et al., 2000) was utilized in CCATT-BRAMS. Land use was provided by the United States Geological Survey (USGS) global 1 km vegetation dataset, updated with a land cover map for the Brazilian Legal Amazon Region for use in meteorological models (PROVEG) (Sestini et al., 2003). PROVEG is based on the Thematic Mapper (TM) Landsat images with spatial resolution of 90 m × 90 m from the year 2000 and deforestation data from the Amazon Deforestation Monitoring Program (PRODES) for the year 1997. For WRF-Chem, albedo and greenness fraction were calculated offline using the updated vegetation dataset, Moderate Resolution Imaging Spectroradiometer (MODIS) Normalized Difference Vegetation Index (NDVI) data from the year 2002–2002 and vegetation parameters from the LEAF-2 land surface model as implemented in CCATT-BRAMS.

Emissions were generated with PREP-CHEM-SRC (Freitas et al., 2011) Version 1.2. Fire emissions were estimated from GOES, AVHRR and MODIS fire count data,

14020

using the Brazilian Biomass Burning Emission Model (3BEM; Longo et al., 2009). Anthropogenic emissions were estimated from the RETRO, GOCART and EDGAR v4.0 global databases updated with South American inventories (Alonso et al., 2010). Biogenic emissions were provided by a monthly climatology for the year 2000 produced with the Model of Emissions of Gases and Aerosols from Nature (MEGAN; Guenther et al., 2006). In WRF-Chem, the same Gaussian diurnal cycle with peak at 15:00 UTC (11:00 LT) is applied to both anthropogenic and biogenic emissions, while in CCATT-BRAMS the diurnal cycle of biogenic emissions follows the solar radiation cycle. In both models, the biomass burning daily cycle peaks at 18:00 UTC (15:00 LT). In both CCATT-BRAMS and WRF-Chem, the Regional Atmospheric Chemistry Mechanism (RACM) was used (Stockwell et al., 1997). In WRF-Chem, the Goddard Chemistry Aerosol Radiation and Transport (GOCART; Chin et al., 2002) aerosol scheme was used with aerosol direct radiative effects. CCATT-BRAMS has a smoke aerosol scheme with intensive optical properties (extinction efficiency, single scattering albedo and asymmetry parameter) calculated in an offline Mie code based on observations of climatological size distribution and complex refractive index from AERONET sites in the southern Amazon (Rosario et al., 2011, 2013). CCATT-BRAMS includes scavenging of soluble species in the convective scheme following Berge (1993), as described in Freitas et al. (2005), where the wet removal rates are a function of the precipitation rate, liquid water content and precipitable water. In the cloud microphysics scheme the wet deposition follows Barth et al. (2001), whereby low solubility species partition into the liquid phase according to Henry's Law and high solubility species by diffusion-limited mass transfer. In WRF-Chem, at the convective-parameterizing scale, a constant fraction of gas and aerosol species in convective updrafts are removed (complete removal for sulfur dioxide – SO_2 , sulfate – H_2SO_4 , ammonium – NH_3 , nitric acid – HNO_3 and sea salt; no removal for hydrophobic organic (OC) and black carbon (BC) and dimethyl sulfide (DMS); and 50% removal for all other aerosol species). On the other hand, no wet scavenging is included for cloud water and precipitation resolved by the microphysics

14021

scheme, because this option is not currently available in WRF-Chem for the RACM chemical mechanism.

The CCATT-BRAMS simulations employ a lightning NO_x parameterization based on convective cloud top height (Stockwell et al., 1999). In WRF-Chem, lightning production of NO_x was not included, because these parameterizations have not yet been evaluated for the Amazon region. Uncertainties remain about the scavenging efficiencies of soluble species by deep convective storms. Simulations of an idealized thunderstorm by several cloud-resolving models yielded varying results for CH_2O , H_2O_2 and HNO_3 in convective outflow due to differing microphysics and assumptions about retention of chemical species during cloud drop freezing (Barth et al., 2007). In the tropics, over continents, lightning production is comparable to other sources of NO_x , including biomass burning and soil release, and it is the primary source over oceans (Bond et al., 2002). Since lightning NO_x production peaks in the upper troposphere, it could be an important contributor to ozone production. The impact of wet deposition and lightning NO_x production on O_3 distributions will be more closely examined in future modeling studies of tropospheric chemistry in the Amazon.

For model results evaluation, the mean vertical O_3 profiles for observations, CCATT-BRAMS and WRF-Chem were calculated for the regions to the west, north, south, east, and around Manaus. Horizontal flight legs were excluded from analysis to eliminate the influence of plumes in the boundary layer. To calculate the mean simulated profiles, the four grid points closest in latitude and longitude to each observation were determined at the two model hours that bracket the observations. At each of these grid points and hours, vertical profiles were extracted from the model output and then linearly interpolated to the observed GPS height. The four points from each time were averaged, weighting by the inverse distance to the observed longitude and latitude. Finally, the prior and posterior hour values were averaged with appropriate weights. Thus, 16 model points were used with spatial and temporal weights to obtain each model value for comparison to observations. The observed and model time series were then separated into five regions to the west, north, east, and south of Manaus, and in the region of

14022

Manaus itself. The mean value and standard deviation were calculated for each region and 500 m vertical bin.

3 Results and discussion

3.1 BARCA O₃ observations

5 The vertical distributions of O₃ measured by the aircraft during BARCA A and B are depicted in Fig. 2. Observations during the dry-to-wet transition (BARCA A) are plotted separately for clean (west, north and around Manaus regions) and fire-influenced polluted (east and south regions) conditions. The O₃ distributions are similar during BARCA A in the clean regions and BARCA B, with median values ranging from 10–
10 25 ppb. However, there is more variability, as measured by the difference between the 25th and 75th percentiles, in the BARCA A data. This may be due to downward mixing of O₃ transported long-range from fires in Africa or recirculated from the polluted southeast Brazil region. In the fire-influenced regions during BARCA A, medians range from 25–45 ppb, peaking at a typical plume injection height for savanna fires of 2–3 km.
15 The highest variability is seen in polluted conditions during BARCA A, particularly at 2–3 km, indicating the influence of small-scale fire plumes. This variability of O₃ in the PBL presents a challenge to the regional models, since the effects of small-scale processes such as plume rise and convection are parameterized and averaged across the grid cell.

20 3.2 Observed and simulated meteorology

In addition to surface emissions and chemical sources and sinks of O₃, several meteorological processes are key drivers of tropospheric O₃ distributions, including solar radiation, tracer transport and removal. Thus, first we evaluate the ability of the models to represent these processes and their seasonalities.

14023

In the dry-to-wet transition season, a band of increased precipitation extends in TRMM 3B43 observations from the northwest Amazon to southeast Brazil, and precipitation is also intense in the ITCZ at 10° N (Fig. 4). In the wet-to-dry transition season, increased precipitation extends from the western Amazon to the northeast coast
5 of Brazil (Fig. 5). Incident solar radiation is higher in the dry than wet season for both sites (Figs. 6–8). At the forest and pasture sites, peak sensible heat flux is higher in the dry-to-wet than wet-to-dry transition seasons, and higher at forest than pasture sites for both seasons, while latent heat flux is higher in the wet-to-dry than dry-to-wet transition seasons for both sites, and higher at the pasture site for both seasons (Figs. 7 and 8).
10 In radiosoundings, a decrease in dew point temperature is observed in upper levels (300–400 hPa) from 0 to 12 or 18 Z, likely due to precipitation, more pronounced in the wet-to-dry transition season (Figs. 9 and 10).

Mean precipitation during the dry-to-wet (November 2008) and wet-to-dry (May 2009) transition seasons was calculated for the TRMM 3B43 data and the CCATT-
15 BRAMS and WRF-Chem models for three regions: the Amazon (15° S–10° N, 50–80° W), northeast Brazil (15° S–0° N, 35–50° W), and southeast South America (15–35° S, 35–65° W). The values are listed in Table 2. The mean precipitation on the 35 km resolution domain for the two months is shown in Figs. 3 and 4, respectively, as well as the delineations of the subregion boxes. The signs of NE–SE differences are correctly modeled by both models during both seasons, i.e., the NE is drier than the SE during November and vice-versa during May. For the Amazon, CCATT-BRAMS slightly underestimates the precipitation rates in both seasons, but the rate in WRF-Chem is about twice that of TRMM 3B43. The models were also evaluated against TRMM 3B42 3 hourly precipitation rates at the 78 surface station locations in the Amazon (Table 3).
20 Both models had a positive bias in both seasons, but WRF-Chem had a higher bias and RMSE than CCATT-BRAMS.

In the dry-to-wet transition season, for both CCATT-BRAMS and WRF-Chem, the mean daily cycle of surface incident shortwave radiation calculated for the Manaus AERONET site for October–November 2008, falls within one standard deviation of

14024

the mean AERONET observations (Fig. 6), but is closer to the upper limit, possibly due to underestimated cloudiness or AOD in the models. For the forest and pasture sites, both models represent the daily cycles of incident shortwave and ingoing and outgoing longwave radiation, although incident shortwave is slightly overestimated (by 50–100 W m⁻²) at peak (Fig. 7). During the wet-to-dry transition season, both models overestimate peak incident shortwave radiation by about 100 W m⁻² (Fig. 8), suggesting that they underestimate cloudiness.

In the dry-to-wet transition season (Fig. 7), the peak latent heat flux at 13:00 LT is higher at the forest site than at the pasture site (460 W m⁻² vs. 268 W m⁻²) whereas the sensible heat flux shows an opposite difference (180 vs. 215 W m⁻²), due to lower evapotranspiration and higher surface temperatures in the pasture. As a result, the observed Bowen ratio (sensible/latent heat flux) is lower at the forest site than the pasture site (0.23–0.38 vs. 0.8). However, in WRF-Chem, the Bowen ratio at 13:00 LT shows a smaller contrast between the forest and pasture sites (0.40 vs. 0.51), due to underestimated sensible heat flux at the pasture site. In the wet-to-dry transition season (Fig. 8), as for the dry-to-wet transition, peak latent heat flux at 13:00 LT is higher at the forest site than at the pasture site (401 W m⁻² vs. 324 W m⁻²). However, the sensible heat flux is also higher at the pasture site (119 W m⁻² vs. 168 W m⁻²) and Bowen ratio is lower at both forest and pasture sites for this season (0.18–0.39 vs. 0.33–0.59). On the other hand, in WRF-Chem, latent and sensible heat flux and thus the Bowen ratio are nearly constant at the forest and pasture sites (0.39 vs. 0.38).

Mean vertical profiles at Manaus from radiosoundings, CCATT-BRAMS and WRF-Chem for October–November 2008 at 0, 12 and 18Z and April–May 2009 at 0 and 12Z are shown in Figs. 9 and 10. For BARCA A, while the temperature profile is well represented by the models, the dew point temperature in CCATT-BRAMS is approximately 10 K too high above 500 hPa and 5 K too low below 500 hPa. The wind speed is overestimated by both models above 500 hPa and underestimated below 500 hPa. For BARCA B, dew point temperature is about 5 K too high in CCATT-BRAMS above 500 hPa. Wind speed is about 2 m s⁻¹ too low above 600 hPa in both models.

14025

The models were evaluated against data from 26 METAR (airports) and 52 Synop (INPE) surface meteorological stations, whose locations are depicted in Fig. 11. Values of Root Mean Squared Error (RMSE) and bias for various meteorological parameters for CCATT-BRAMS and WRF-Chem simulations for BARCA A (October–November 2008) and BARCA B (April–May 2009) are shown in Table 3. Both models overestimate precipitation on average, with a RMSE of 2.4–3.0 mm h⁻¹ and bias of 0.3–3.5 mm h⁻¹ for CCATT-BRAMS, and RMSE of 4.5–7.1 mm h⁻¹ and bias of 3.5–5.8 mm h⁻¹ for WRF-Chem. Dew point temperature is underestimated by 1–2 K and surface pressure is underestimated by 1–2 hPa. Wind speed is underestimated by CCATT-BRAMS and overestimated by WRF-Chem by 0.1–0.6 m s⁻¹. Temperature is underestimated in all cases by 0.1–2.4 K except by CCATT-BRAMS during BARCA A, which overestimated temperature by about 1 K.

Now we summarize the key findings of the model-data meteorological comparison and their implications for the chemistry simulations. The models capture the seasonal spatial distribution of precipitation over northern South America, although the mean precipitation rates are slightly lower (CCATT-BRAMS) and substantially higher (WRF-Chem) than the TRMM retrievals in the Amazon region. This may indicate errors in the strength and vertical distribution of convective transport and the amount of convective wet removal. Peak shortwave radiation is slightly overestimated by both models, which may be related to low cloudiness (convection is triggering too early) or AOD (too much aerosol wet removal). This will increase O₃ production from photolysis, as well as increase surface temperature and evaporation. Although biogenic emissions are not coupled with meteorology in these simulations, this may increase biogenic emissions in future studies that include online biogenic emissions. WRF-Chem predicts a nearly constant Bowen ratio at forest and pasture sites. This indicates that the Noah land surface model is not properly representing the impact of conversion of forest to pasture and the resulting increase in sensible heat flux. The models generally show good agreement with soundings, but excess moisture in CCATT-BRAMS above 500 hPa may stimulate excess O₃ production. Despite these limitations, the models

14026

are able to capture the meteorological contrast between the dry-to-wet and wet-to-dry transition seasons.

3.3 Observed and simulated chemistry

5 Lower levels of O_3 in the rainy season are largely associated with increased presence of convective clouds and precipitation. Decreased surface temperatures and incident solar radiation due to cloudiness suppress emissions of biogenic VOCs such as isoprene. In addition, higher surface humidity and precipitation decrease the occurrence of fires that emit NO_x and VOCs. O_3 precursors are further decreased by wet removal within the storms. On the other hand, during the dry-to-wet transition season, increased
10 solar radiation, latent heat and temperature stimulate the production of OH and other HO_x radicals that can stimulate net O_3 production.

For BARCA, the simulated mean monthly emission rates for two O_3 precursors, NO_x (anthropogenic and biomass burning) and isoprene (biogenic) are shown in Fig. 12. In November 2008, elevated NO_x emission rates of up to $5 \times 10^{-5} \text{ kg m}^{-2} \text{ d}^{-1}$ are seen
15 from an area of intense biomass burning in the northeast Amazon, as well as from more scattered fires in the southeast Amazon. These are both regions that were overflowed by the aircraft (Fig. 12). In May 2009, the Amazon region is largely free of fire. Because biogenic NO emissions (e.g., from soil) were not included in the MEGAN climatology used in this study, background NO emissions (in absence of fire) are likely too low.
20 Typical model anthropogenic NO_x emissions values over the Amazon, primarily from biofuel sources, were $0.008\text{--}13 \mu\text{g N m}^{-2} \text{ h}^{-1}$ N. These NO_x emissions included in the models were less than one third of the mean values of $44 \pm 14 \mu\text{g N m}^{-2} \text{ h}^{-1}$ NO measured by Kaplan et al. (1988) during ABLE-2A. This is considered a threshold value for
25 NO_x -driven O_3 production to be the dominant O_3 source in the PBL. The model emissions were also much lower than the mean emissions from forest of $35.8 \mu\text{g N m}^{-2} \text{ h}^{-1}$ NO measured in the 1998 dry season (Garcia-Montiel et al., 2003). Wetting the forest soil resulted in small pulses of NO and therefore the mean emissions are expected

14027

to be higher in the wet season than dry season. Isoprene emissions are highest in the western and southern Amazon, reaching $15 \times 10^{-5} \text{ kg m}^{-2} \text{ d}^{-1}$ in November 2008 and $5\text{--}10 \times 10^{-5} \text{ kg m}^{-2} \text{ d}^{-1}$ in the aircraft sampling region. Due to decreased surface
5 temperature and incident solar radiation in the rainy season, isoprene emissions in the Amazon Basin are much lower during BARCA B, $3\text{--}5 \times 10^{-5} \text{ kg m}^{-2} \text{ d}^{-1}$. The MEGAN emissions are consistent with isoprene emission measurements above the Amazonian canopy: a normalized flux of $5.76 \times 10^{-5} \text{ kg m}^{-2} \text{ d}^{-1}$ in July 2000 at the end of the rainy season (Rinne et al., 2002) and an average noontime flux of $18.7 \pm 5.5 \times 10^{-5} \text{ kg m}^{-2} \text{ d}^{-1}$
10 in September 2004 during the dry season (Karl et al., 2007).

Figures 13 and 14 show the average O_3 dry deposition flux and median daytime deposition velocity, respectively, as simulated on the 35 km resolution domain by the CCATT-BRAMS and WRF-Chem models for November 2008 and May 2009. In the Amazon Basin, O_3 deposition fluxes are higher in the dry-to-wet transition season, with values reaching $3.5 \text{ nmol m}^{-2} \text{ s}^{-1}$ for CCATT-BRAMS and $6 \text{ nmol m}^{-2} \text{ s}^{-1}$ for WRF-Chem in the northeast Amazon, near the region of concentrated biomass burning.
15 These values are also seen along the northern Andes and southeast Brazil, due to recirculation of O_3 -rich air. In the wet-to-dry transition season, O_3 deposition is at a minimum in the western Amazon, with values of $0.5\text{--}1 \text{ nmol m}^{-2} \text{ s}^{-1}$ for CCATT-BRAMS and $2 \text{ nmol m}^{-2} \text{ s}^{-1}$ for WRF-Chem. For both models, deposition velocities are higher
20 over the rainforest than in the savanna to the east or south of the Amazon Basin, and higher in the wet-to-dry transition than in the dry-to-wet transition. These patterns are also seen in the tower observations in Table 4.

O_3 surface fluxes and dry deposition velocities predicted by the models were compared with observations from several field campaigns (Table 4). These include during the dry (May 1999) and wet (September–October 1999) seasons at Reserva Biológica Jarú (RBJ, forest) and Fazenda Nossa Senhora (FNS, pasture) from LBA-EUSTACH (Rummel et al., 2009; Kirkman et al., 2002) and during the wet season at Reserva Ducke (RD, forest tower near Manaus, 2.95° S , 59.95° W) from ABLE 2B (April–May 1987) (Fan et al., 1990) and at FNS from LBA-TRMM (January–February 1999) (Sigler
25

14028

et al., 2002). For the observations, the means of the hourly (WRF-Chem) and 3 hourly (CCATT-BRAMS) O_3 dry deposition fluxes ($\text{nmol m}^{-2} \text{s}^{-1}$) and the medians of the day-time (11:00–21:00 UTC) hourly mean deposition velocities (cm s^{-1}) are shown. The values were extracted from the grid points closest to the tower locations. In the observations, O_3 fluxes are larger in the dry season, due to higher O_3 mixing ratios. However, deposition velocities are higher in the wet season, and O_3 deposition to the Amazon forest constitutes a globally significant O_3 sink (Rummel et al., 2009). Both models capture these patterns, but the models underestimate the deposition velocities by 15–75 %, which may be partially responsible for the low O_3 fluxes at the Jarú forest site in both seasons and the pasture site in the dry season.

The mean tropospheric and total tropospheric column O_3 from OMI/MLS, CCATT-BRAMS and WRF-Chem for November 2008 and May 2009 are shown in Figs. 15 and 16, respectively. The models significantly underestimate the total columns from satellite and middle altitudes from BARCA. For both BARCA A and B, the models represent the pattern of lower O_3 over the Amazon and higher values over northeast Brazil (BARCA A only) and at 30°S , although the values are strongly underestimated. In November 2008, OMI/MLS mean tropospheric O_3 concentrations show an inflow of elevated O_3 (mean ca. 55 ppb, total 40–45 DU) on the northeast Brazilian coast due to cross-Atlantic transport from biomass burning in southern and sub-Saharan Africa. Additionally, a band of elevated O_3 (mean 55–60 ppb, total 35–40 DU) passes over the South American continent at around 30°S , also from cross-Atlantic transport. During this month, Northern Hemisphere O_3 levels to the north of South America are relatively low (mean 35–40 ppb, total 25–30 DU). On the other hand, the tropospheric ozone distribution in May 2009 (Fig. 16) is characterized by a band of low ozone extending over the Amazon Basin and northeast Brazil between 10°S and 10°N (mean 25–35 ppb, total 20–25 DU). In addition, lightly elevated values are found at around 30°S , primarily over the oceans (40–55 ppb, 30–35 DU) and higher ozone in the Northern Hemisphere (mean 50–55 ppb, total 35–40 DU to the north of 10°N). Both models capture

14029

the overall distribution (inflow in NE Brazil in November 2008, lower values over the Amazon Basin, elevated at 30°S) but values are underestimated relative to OMI/MLS.

However, the BARCA observations are generally lower than the models in the boundary layer, indicating that the satellites appear here to be dominated by the middle troposphere and long-range transport. An example of observed and simulated O_3 during the flight legs between Manaus and Belém in BARCA A and B is shown in Fig. 17. While the models capture the pattern of increasing O_3 values with height, the models underestimate elevated O_3 values from 2.5–4.5 km, and overestimate low values near the surface (1–1.5 km). The models also do not reproduce the variability in the high values, likely due to the aircraft intersection of biomass burning plumes. This is expected given the coarse horizontal grid resolution. Thus, mean profiles are analyzed in order to study differences among the regions and seasons and to assess the models' abilities to capture the impacts of such small-scale processes on regional O_3 distributions.

The mean vertical O_3 profiles for observations, CCATT-BRAMS and WRF-Chem for the regions to the west, north, south, east and around Manaus are shown for BARCA A and B in Figs. 18 and 20, respectively, and NO profiles corresponding to the aircraft tracks are depicted in Figs. 19 and 21, respectively. Mean profiles from longitudinal surveys over Amazônia of O_3 during ABLE-2A (Browell et al., 1988) and ABLE-2B (Harris et al., 1990) and NO during ABLE-2A (Torres and Buchan, 1988) are included for comparison. In BARCA B, O_3 values were at or near background values in all regions, ranging from 8–15 ppb at the surface to 2–15 ppb at 4–4.5 km, and the models are generally within 5–10 ppb of the observations. During BARCA A, while the W region still had low O_3 values (5 ppb at the surface to 20 ppb at 4–4.5 km), the N, S and M regions ranged from 15–20 ppb at the surface to 30–35 ppb at 4–4.5 km, and the E region presented the most elevated values, from 25–55 ppb. ABLE-2A O_3 profiles are similar in all regions, ranging from 15–20 ppb near the surface to 30–40 ppb from 4–6 km, so that the BARCA values are higher in the fire-influenced east and south regions, lower in the north and west regions, and very similar around Manaus. The profiles from ABLE-2B are within one standard deviation of the BARCA B measurements, except for the north

14030

region, where they are lower (5–15 ppb). These results suggest an increasing influence of fire emissions to the east and south of Manaus, but that O_3 in clean regions has not changed much.

Both models generally overestimate O_3 from 1–2 km and underestimate O_3 from 3–4.5 km. As seen in the CO results shown in Andreae et al. (2012), the model profiles have steeper slopes than the observations, except in the polluted south, possibly due to excessive vertical mixing of precursors. In addition, the models may be missing sources of O_3 and/or precursors at 3–4.5 km in the model inflow boundary conditions. In general the models overestimate O_3 in the PBL compared to aircraft measurements, but underestimate the total column values relative to the OMI/MLS satellite product. This suggests that the total column values in Amazonia are dominated by global pollution from Africa, rather than local O_3 production from biomass burning. A typical OMI averaging kernel (cloud-free ocean conditions) shows maximum sensitivity from 594–416 hPa (Zhang et al., 2010). Therefore, OMI may not be detecting O_3 in the PBL from local sources, but rather primarily seeing global pollution from Africa.

The excess O_3 in the PBL in the models could be due to either a low deposition sink, as O_3 dry deposition velocities in the models are about half of observed values, or excessive model sensitivity to NO_x emissions, or both. Two additional simulations were conducted with WRF-Chem to evaluate the model sensitivity to these processes: (1) doubling the calculated deposition velocity for O_3 only (2DEPVEL) and (2) halving the NO_x surface emission rates (0.5ENOX). The O_3 profiles corresponding to BARCA flights for these two simulations are also included in Figs. 18 and 20. The corresponding NO profiles from all model simulations as well as a mean profile over Amazonia from ABLE-2A are depicted in Figs. 19 and 21. The 0.5ENOX simulation reduces O_3 more than 2DEPVEL throughout the entire profile. In the dry-to-wet transition, 2DEPVEL reduces O_3 in the lower PBL by about 25 %, while 0.5ENOX decreases O_3 by around 40 %, and in the wet-to-dry-transition the reductions are about 10 and 30 %, respectively. In general the 0.5ENOX O_3 profiles are lower than observed in the first 500 m above the surface, but they provide the best representation of the data for the

14031

north and west regions in the dry-to-wet transition. They also provide a similarly good fit as 2DEPVEL for the east, Manaus and south regions, while in the wet-to-dry transition 0.5ENOX is closer to the observed value from 0–500 m in all regions except the north. During BARCA A, NO in all WRF-Chem simulations in the north, west, and Manaus regions is 10–15 ppt from 0–500 m above the surface, increasing to a maximum of 20–50 ppt at 2 km a.g.l., and is generally lower than the ABLE-2A observations in the PBL. In the east and south, where biomass burning influence was seen, NO in 0–500 m a.g.l. increased from 20–50 ppt in the base simulation to 35–60 ppt in 2DEPVEL due to decreased O_3 and conversion of NO to NO_2 , and was generally within one standard deviation of the ABLE-2A measurements in the PBL. In BARCA B, NO simulated by WRF-Chem is very low, 5–10 ppt in the entire profile, except for the west region, where a mean NO of 30 ppt is seen from 0–500 m a.g.l. This is again due to very low O_3 , and for the Manaus region, where anthropogenic NO_x sources may have contributed to NO values of 20 ppt. These results suggest that adjustment of dry deposition parameterizations are needed to increase O_3 deposition velocities by about a factor of two in agreement with ground observations. Future research will compare simulated NO_x fields with observations from more recent field campaigns, as the results of these simulations also suggest that O_3 in WRF-Chem is very sensitive to NO_x emissions.

Above the boundary layer, from 3–4 km a.g.l., chemical inflow at the eastern boundary of South America may contribute to O_3 elevated above background. In order to evaluate the model representation of this inflow, vertical profiles from SHADOZ soundings on the northeast coast of South America during the BARCA A and B periods were compared with CCATT-BRAMS and WRF-Chem (Fig. 22). In addition, 120 h back trajectories from the sounding locations at heights of 1500 m, 6000 and 9000 m above ground level (gal) were calculated with the HYSPLIT model (<http://ready.arl.noaa.gov/hypub-bin/trajtype.pl?runtype=archive>) using meteorological data from the NCEP/NCAR global reanalysis. Inflow at Paramaribo originated either in the Caribbean or the tropical Atlantic, while at Natal, air parcels came from anti-cyclonic

14032

recirculation from southeastern Brazil or the tropical Atlantic. Both models generally represent the SHADOZ O_3 profiles up to 600 hPa, but do not capture layers of elevated O_3 above 500 hPa. These are likely to be either from pollution recirculated from southeast Brazil or possibly from African biomass burning. The models also do not reproduce thinner layers of high O_3 below 600 hPa. For example, at Natal on November 7, 2008 (Fig. 22c, air of African origin at ~ 850 hPa and ~ 470 hPa) and November 19, 2008 (Fig. 22d, air from the central African coast at ~ 850 hPa and recirculation from southeastern Brazil at ~ 470 hPa and ~ 310 hPa) and at Paramaribo on 11 May 2009 (Fig. 22f, air of tropical Atlantic origin at all three levels), both models underestimate O_3 above 500 hPa by 40–60 ppb (model values of 30–50 ppb vs. observations maximum values of 80–100 ppb). A previous analysis of ozone soundings and aircraft measurements at Natal suggested that increases in tropospheric ozone in the Southern Hemisphere springtime may be due to stratospheric intrusion (Logan, 1985). This is consistent with the November 2008 profiles at Natal; the models may not be capturing the intrusion of stratospheric air masses seen in the observations, indicated by upper tropospheric (> 500 hPa) layers with elevated O_3 and very low relative humidity ($< 20\%$). On the other hand, at Paramaribo on November 6 and November 25, 2008 and at Paramaribo on 4 May 2009, when air masses at all levels were of Northern Hemisphere origin, the models reproduced the nearly constant with altitude O_3 values of 30–40 ppb.

In summary, chemistry simulations of the BARCA periods with CCATT-BRAMS and WRF-Chem overestimated O_3 in the PBL by 5–10 ppb in the wet-to-dry transition (BARCA B), with background levels observed (10–20 ppb) in all regions. In the dry-to-wet transition (BARCA A), the models generally reproduced elevated O_3 levels in the northeast and southeast Amazon where biomass burning emissions of precursors led to significant enhancements of ambient O_3 . The models overestimate O_3 in the PBL by 5–10 ppb, whereas from 2–4 km the modeled values are generally lower than observations. These discrepancies of models with observations may result from an overly-mixed (constant with altitude) profile due to overly active vertical mixing from

14033

the PBL scheme from 1–2 km or too much downward convective transport of O_3 from 2 km to the surface, as observed by Betts et al. (2002). In the lower boundary layer, the surface sink of O_3 (dry deposition) may be too low, or overestimation of NO_x sources may produce too much O_3 . Additional simulations with WRF-Chem showed that O_3 in the lower boundary layer was about twice as sensitive to increases in O_3 deposition velocity as reductions in NO_x emissions, but both simulations achieved better agreement with observations. Although NO emissions over the forest were less than half of observed values, likely due to the lack of inclusion of soil emissions, sufficient O_3 production occurred to match or exceed aircraft observations, suggesting that the model chemistry is overly NO_x -sensitive.

4 Conclusions

The BARCA campaign offered the first regional aircraft survey of O_3 in the Amazon Basin in both the dry-to-wet and wet-to-dry transition seasons. In both seasons, extremely low background O_3 values (< 20 ppb) were observed to the west and north of Manaus, and in the wet-to-dry transition low O_3 was also measured to the east and south and in the region around Manaus. These background values are the lowest observed on Earth, due to a combination of isolation from anthropogenic and biomass burning NO_x sources and O_3 deposition to the forest canopy, and the ecosystem and atmospheric chemistry is adjusted to these very low values. According to the models, the chemistry in the Amazon is very sensitive to NO_x emissions from soils, so that even a small overestimate of NO_x emissions generates too much O_3 in the PBL. However, it is likely that the model chemistry is incorrect in the PBL, because the models have about the right amount of NO_x but far too much O_3 in the PBL. Therefore, we conclude that the current model chemistry produces much more O_3 per unit NO_x than the atmosphere at very low NO_x , but may be about right in polluted conditions. Further simulations with WRF-Chem showed that the model O_3 production is very sensitive to both the O_3 deposition velocities, which were about one half of observed values,

14034

and the NO_x emissions. In addition, simulated O_3 was lower than both the OMI/MLS total tropospheric O_3 and the BARCA observations in mid-levels, indicating that the O_3 retrieved by satellites is dominated by the middle troposphere and long-range transport and does not represent well boundary layer O_3 values. As the regional population grows in the Amazon basin, leading to increases in both urban and fire NO_x sources, this is indeed a big concern because PBL O_3 is lower in clean areas than the models predict, so that the change to polluted conditions is larger, and that the chemistry to define the path to higher NO_x conditions is poorly represented. Future modeling studies can include more complete organic chemistry and biogenic emissions, including NO emissions from soil, as well as improved representation of lightning NO_x production, dry deposition, convective transport and wet scavenging processes, to address this NO_x sensitivity. Additionally, future field campaigns in the Amazon that include aircraft observations of nitrogen oxides and hydrocarbons and ground-based measurements of NO flux from the forest canopy may allow better constraints on the Amazonian O_3 budget.

Acknowledgements. The authors are grateful to the entire BARCA team, including E. Gottlieb, V. Y. Chow, M. D. P. Longo, G. W. Santoni, F. Morais, A. C. Ribeiro, N. Jürgens, J. Steinbach, H. Chen, O. Kolle, L. V. Gatti, J. B. Miller, and the two INPE Bandeirante airplane pilots, P. Celso and D. Gramacho. We would also like to thank the GMAI group at INPE for indispensable support with the modeling and analysis, including F. Santos, R. Stockler, R. Mello, M. Alonso, M. Sanchez, D. Franca, R. Braz, H. Lopez, and V. Oliveira. Many thanks to A. Thompson, N. Paes Leme, R. Scheele, and F. J. Schmidlin for the SHADOZ ozone sounding data. We thank B. Holben for his effort in establishing and maintaining the Manaus AERONET site. This work was supported by an IIE Fulbright Scholarship and PCI CNPQ, and the flight campaign was supported by the Max Planck Society, NASA grants NASA NNX08AP68A and NASA NNX10AR75G, FAPESP thematic project AEROCLIMA 2008/58100-2, CNPq Millennium Institute of the Large Scale Biosphere – Atmosphere Experiment in Amazonia (LBA) (CNPq Project 477575/2008-0), and MCT and INPE.

14035

References

- Alonso, M. F., Longo, K., Freitas, S., Fonseca, R., Marecal, V., Pirre, M., and Klenner, L.: An urban emissions inventory for South America and its application in numerical modeling of atmospheric chemical composition at local and regional scales, *Atmos. Environ.*, 44, 5072–5083, 2010.
- Andreae, M. O., Artaxo, P., Fischer, H., Freitas, S. R., Grégoire, J.-M., Hansel, A., Hoor, P., Kormann, R., Krejci, R., Lange, L., Lelieveld, J., Lindinger, W., Longo, K., Peters, W., de Reus, M., Scheeren, B., Silva Dias, M. A. F., Stroem, J., van Velthoven, P. F. J., and Williams, J.: Transport of biomass burning smoke to the upper troposphere by deep convection in the equatorial region, *Geophys. Res. Lett.*, 28, 951–954, 2001.
- Andreae, M. O., Artaxo, P., Brandão, C., Carswell, F. E., Ciccioli, P., da Costa, A. L., Culf, A. D., Esteves, J. L., Gash, J. H. C., Grace, J., Kabat, P., Lelieveld, J., Malhi, Y., Manzi, A. O., Meixner, F. X., Nobre, A. D., Nobre, C., Ruivo, M. D. L. P., Silva-Dias, M. A., Stefani, P., Valentini, R., von Jouanne, J., and Waterloo, M. J.: Biogeochemical cycling of carbon, water, energy, trace gases, and aerosols in Amazonia: the LBA-EUSTACH experiments, *J. Geophys. Res.*, 107, 8066, doi:10.1029/2001JD000524, 2002.
- Andreae, M. O., Rosenfeld, D., Artaxo, P., Costa, A. A., Frank, G. P., Longo, K. M., Silva Dias, M. A. F.: Smoking rain clouds over the Amazon, *Science*, 303, 1337–1342, 2004.
- Andreae, M. O., Artaxo, P., Beck, V., Bela, M., Freitas, S., Gerbig, C., Longo, K., Munger, J. W., Wiedemann, K. T., and Wofsy, S. C.: Carbon monoxide and related trace gases and aerosols over the Amazon Basin during the wet and dry seasons, *Atmos. Chem. Phys.*, 12, 6041–6065, doi:10.5194/acp-12-6041-2012, 2012.
- Avery, M., Twohy, C., McCabe, D., Joiner, J., Severance, K., Atlas, E., Blake, D., Bui, T. P., Crounse, J., Dibb, J., Diskin, G., Lawson, P., McGill, M., Rogers, D., Sachse, G., Scheuer, E., Thompson, A. M., Trepte, C., Wennberg, P., and Ziemke, J.: Convective distribution of tropospheric ozone and tracers in the Central American ITCZ region: evidence from observations during TC4, *J. Geophys. Res.*, 115, D00J21, doi:10.1029/2009JD013450, 2010.
- Barth, M. C., Stuart, A. L., and Skamarock, W. C.: Numerical simulations of the July 10 STERAO/Deep Convection storm: Redistribution of soluble tracers, *J. Geophys. Res.*, 106, 12381–12400, 2001.
- Barth, M. C., Kim, S.-W., Wang, C., Pickering, K. E., Ott, L. E., Stenchikov, G., Leriche, M., Cautenet, S., Pinty, J.-P., Barthe, Ch., Mari, C., Helsdon, J. H., Farley, R. D., Fridlind, A. M.,

14036

- Ackerman, A. S., Spiridonov, V., and Telenta, B.: Cloud-scale model intercomparison of chemical constituent transport in deep convection, *Atmos. Chem. Phys.*, 7, 4709–4731, doi:10.5194/acp-7-4709-2007, 2007.
- Beck, V., Gerbig, C., Koch, T., Bela, M. M., Longo, K. M., Freitas, S. R., Kaplan, J. O., Prigent, C., Bergamaschi, P., and Heimann, M.: WRF-Chem simulations in the Amazon region during wet and dry season transitions: evaluation of methane models and wetland inundation maps, *Atmos. Chem. Phys.*, 13, 7961–7982, doi:10.5194/acp-13-7961-2013, 2013.
- Berge, E.: Coupling of wet scavenging of sulphur to clouds in a numerical weather prediction model, *Tellus B*, 45, 1–22, 1993.
- Betts, A. K., Gatti, L. V., Cordova, A. M., Silva Dias, M. A. F., and Fuentes, J. D.: Transport of ozone to the surface by convective downdrafts at night, *J. Geophys. Res.*, 107, 8046, doi:10.1029/2000JD000158, 2002.
- Bond, D. W., Steiger, S., Zhang, R., Tie, X. X., and Orville, R. E.: The importance of NO_x production by lightning in the tropics, *Atmos. Environ.*, 36, 1509–1519, doi:10.1016/S1352-2310(01)00553-2, 2002.
- Browell, E. V., Gregory, G. L., Harriss, R. C., and Kirchhoff, V. W. J. H.: Tropospheric ozone and aerosol distributions across the Amazon Basin, *J. Geophys. Res.*, 93, 1431–1451, doi:10.1029/JD093iD02p01431, 1988.
- Browell, E. V., Fenn, M. A., Butler, C. F., Grant, W. B., Clayton, M. E., Fishman, J., Bachmeier, A. S., Anderson, B. E., Gregory, G. L., Fuelberg, H. E., Bradshaw, J. D., Sandholm, S. T., Blake, D. R., Heikes, B. G., Sachse, G. W., Singh, H. B., and Talbot, R. W.: Ozone and aerosol distributions and air mass characteristics over the South Atlantic Basin during the burning season, *J. Geophys. Res.*, 101, 24043–24068, 1996.
- Buarque, D. C., de Paiva, R. C. D., Clarke, R. T., and Mendes, C. A. B.: A comparison of Amazon rainfall characteristics derived from TRMM, CMORPH and the Brazilian national rain gauge network, *J. Geophys. Res.*, 116, D19105, doi:10.1029/2011JD016060, 2011.
- Chin, M., Ginoux, P., Kinne, S., Holben, B. N., Duncan, B. N., Martin, R. V., Logan, J. A., Higurashi, A., and Nakajima, T.: Tropospheric aerosol optical thickness from the GOCART model and comparisons with satellite and sunphotometer measurements, *J. Atmos. Sci.*, 59, 461–483, 2002.
- Cordova Leal, A. M.: Gases Traço na Amazônia: Variabilidade Sazonal e Temporal de O₃, NO_x e CO em Ambientes de Pastagem e Floresta, Tese de Doutorado, Instituto de Astronomia, Geofísica e Ciências Atmosféricas da Universidade de São Paulo, 2003.

14037

- Crutzen, P. J., Delany, A. C., Greenberg, J. P., Haagenson, P., Heidt, L., Lueb, R., Pollock, W., Seiler, W., Wartburg, A. F., and Zimmerman, P. R.: Tropospheric chemical composition measurements in Brazil during the dry season, *J. Atmos. Chem.*, 2, 233–256, 1985.
- Ebben, C. J., Martinez, I. S., Shrestha, M., Buchbinder, A. M., Corrigan, A. L., Guenther, A., Karl, T., Petäjä, T., Song, W. W., Zorn, S. R., Artaxo, P., Kulmala, M., Martin, S. T., Russell, L. M., Williams, J., and Geiger, F. M.: Contrasting organic aerosol particles from boreal and tropical forests during HUMPPA-COPEC-2010 and AMAZE-08 using coherent vibrational spectroscopy, *Atmos. Chem. Phys.*, 11, 10317–10329, doi:10.5194/acp-11-10317-2011, 2011.
- Fan, S. M., Wofsy, S. C., Bakwin, P. S., Jacob, D. J., and Fitzjarrald, D. R.: Atmosphere-biosphere exchange of CO₂ and O₃ in the central Amazon forest, *J. Geophys. Res.*, 95, 16851–16864, 1990.
- Fishman, J. and Larsen, J. C.: The distribution of total ozone and stratospheric ozone in the tropics: implications for the distribution of tropospheric ozone, *J. Geophys. Res.*, 92, 6627–6634, 1987.
- Fueglistaler, S., Dessler, A. E., Dunkerton, T. J., Folkins, I., Fu, Q., and Mote, P. W.: Tropical tropopause layer, *Rev. Geophys.*, 47, RG1004, doi:10.1029/2008RG000267, 2009.
- Freitas, S. R., Silva Dias, M. A. F., Silva Dias, P. L., Longo, K. M., Artaxo, P., Andreae, M. O., and Fischer, H.: A convective kinematic trajectory technique for low-resolution atmospheric models, *J. Geophys. Res.*, 105, 24375–24386, doi:10.1029/2000JD900217, 2000.
- Freitas, S., Longo, K., Silva Dias, M., Silva Dias, P., Chatfield, R., Prins, E., Artaxo, P., Grell, G., and Recuero, F.: Monitoring the transport of biomass burning emissions in South America, *Environ. Fluid Mech.*, 5, 135–167, doi:10.1007/s10652-005-0243-7, 2005.
- Freitas, S. R., Longo, K. M., Chatfield, R., Latham, D., Silva Dias, M. A. F., Andreae, M. O., Prins, E., Santos, J. C., Gielow, R., and Carvalho Jr., J. A.: Including the sub-grid scale plume rise of vegetation fires in low resolution atmospheric transport models, *Atmos. Chem. Phys.*, 7, 3385–3398, doi:10.5194/acp-7-3385-2007, 2007.
- Freitas, S. R., Longo, K. M., Silva Dias, M. A. F., Chatfield, R., Silva Dias, P., Artaxo, P., Andreae, M. O., Grell, G., Rodrigues, L. F., Fazenda, A., and Panetta, J.: The Coupled Aerosol and Tracer Transport model to the Brazilian developments on the Regional Atmospheric Modeling System (CATT-BRAMS) – Part 1: Model description and evaluation, *Atmos. Chem. Phys.*, 9, 2843–2861, doi:10.5194/acp-9-2843-2009, 2009.

14038

- Freitas, S. R., Longo, K. M., Alonso, M. F., Pirre, M., Marecal, V., Grell, G., Stockler, R., Mello, R. F., and Sánchez Gácita, M.: PREP-CHEM-SRC – 1.0: a preprocessor of trace gas and aerosol emission fields for regional and global atmospheric chemistry models, *Geosci. Model Dev.*, 4, 419–433, doi:10.5194/gmd-4-419-2011, 2011.
- 5 Gallardo, L., Alonso, M., Andrade, M. F., Carvalho, V. S. B., Behrentz, E., Vasconcellos, P. C., D'Angiola, A., Dawidowski, L., Freitas, S., Gómez, D., Longo, K. M., Martins, M., Mena, M., Matus, P., Osses, A., Osses, M., Rojas, N., Saide, P., Sánchez-Ccoyllo, O., and Toro, M. V.: South America, in: IGAC Report on Megacity Air Pollution and Climate, World Meteorological Organization, Research Department, Atmospheric Research and Environment Branch, Geneva, 2010.
- 10 Garcia-Montiel, D. C., Steudler, P. A., Piccolo, M., Neill, C., Melillo, J., and Cerri, C. C.: Nitrogen oxide emissions following wetting of dry soils in forest and pastures in Rondônia, Brazil, *Biogeochemistry*, 64, 319–336, 2003.
- Gevaerd, R.: Estudo da Redistribuição 3-D de Gases e Aerossóis de Queimadas em Roraima 1998, Master's thesis, University of São Paulo, 2005.
- 15 Gevaerd, R. and Freitas, S. R.: Estimativa operacional da umidade do solo para iniciação de modelos de previsão numérica da atmosfera, Parte I: Descrição da metodologia e validação, *Revista Brasileira de Meteorologia*, 21, 59–73, 2006.
- Gevaerd, R., Freitas, S., and Longo, K.: Numerical simulation of biomass burning emission and transport during 1998 Roraima fires, in: International Conference on Southern Hemisphere Meteorology and Oceanography (ICSHMO), 8, Proceedings, Foz do Iguaçu, INPE, São José dos Campos, 2006, 883–889, CD-ROM, ISBN 85-17-00023-4, 2006.
- 20 Guenther, A., Karl, T., Harley, P., Wiedinmyer, C., Palmer, P. I., and Geron, C.: Estimates of global terrestrial isoprene emissions using MEGAN (Model of Emissions of Gases and Aerosols from Nature), *Atmos. Chem. Phys.*, 6, 3181–3210, doi:10.5194/acp-6-3181-2006, 2006.
- Grell, G. A. and Dévényi, D.: A generalized approach to parameterizing convection combining ensemble and data assimilation techniques, *Geophys. Res. Lett.*, 29, 38-1–38-4, doi:10.1029/2002GL015311, 2002.
- 30 Grell, G. A., Peckham, S. E., Schmitz, R., McKeen, S. A., Frost, G., Skamarock, W. C., and Eder, B.: Fully coupled online chemistry within the WRF model, *Atmos. Environ.*, 39, 6957–6975, 2005.

14039

- Harriss, R. C., Wofsy, S. C., Garstang, M., Browell, E. V., Molion, L. C. B., McNeal, R. J., Hoell Jr., J. M., Bendura, R. J., Beck, S. M., Navarro, R. L., Riley, J. T., and Snell, R. L.: The Amazon boundary layer experiment (ABLE 2A): dry season 1985, *J. Geophys. Res.*, 93, 1351–1360, doi:10.1029/JD093iD02p01351, 1988.
- 5 Harriss, R. C., Garstang, M., Wofsy, S. C., Beck, S. M., Bendura, R. J., Coelho, J. R. B., Drewry, J. W., Hoell, J. M., Matson, P. A., McNeal, R. J., Molion, L. C. B., Navarro, R. L., Rabine, V., and Snell, R. L.: The Amazon boundary layer experiment: wet season 1987, *J. Geophys. Res.*, 95, 16721–16736, 1990.
- Jacob, D. J. and Wofsy, S. C.: Photochemistry of biogenic emissions over the Amazon forest, *J. Geophys. Res.*, 93, 1477–1486, doi:10.1029/JD093iD02p01477, 1988.
- 10 Janjjae, Z. I.: The step-mountain eta coordinate model: further developments of the 445 convection, viscous sublayer and turbulence closure schemes, *Mon. Weather Rev.*, 122, 446, 927–945, 1994.
- Kaplan, W. A., Wofsy, S. C., Keller, M., and Da Costa, J. M.: Emission of NO and deposition of O₃ in a tropical forest system, *J. Geophys. Res.*, 93, 1389–1395, doi:10.1029/JD093iD02p01389, 1988.
- 15 Karl, T., Guenther, A., Yokelson, R. J., Greenberg, J., Potosnak, M., Blake, D. R., and Artaxo, P.: The tropical forest and fire emissions experiment: Emission, chemistry, and transport of biogenic volatile organic compounds in the lower atmosphere over Amazonia, *J. Geophys. Res.*, 112, D18302, doi:10.1029/2007JD008539, 2007.
- 20 Kaufman, Y., Hobbs, P. V., Kirchhoff, V. W., Artaxo, P., Remer, L., Holben, B. N., King, M. D., Prins, E. M., Ward, D. E., Longo, K. M., Mattos, L. F., Nobre, C. A., Spinhirne, J., Thompson, A. M., Gleason, J. F., and Christopher, S. A.: Smoke, Clouds, and Radiation-Brazil (SCAR-B) experiment, *J. Geophys. Res.*, 103, 31783–31808, doi:10.1029/98JD02281, 1998.
- 25 Kawanishi, T., Kuroiwa, H., Kojima, M., Oikawa, K., Kozu, T., Kumagai, H., Okamoto, K., Okumura, M., Nakatsuka, H., and Nishikawa, K.: TRMM precipitation radar, *Remote Sens. Appl.-Earth Atmos. Oceans*, 25, 969–972, 2000.
- Kirchhoff, V. W. J. H., da Silva, I. M. O., and Browell, E. V.: Ozone measurements in Amazonia: dry season versus wet season, *J. Geophys. Res.*, 95, 16913–16926, 1990.
- 30 Kirkman, G. A., Gut, A., Ammann, C., Gatti, L. V., Cordova, A. M., Moura, M. A. L., Andreae, M. O., and Meixner, F. X.: Surface exchange of nitric oxide, nitrogen diox-

14040

- ide, and ozone at a pasture in Rondonia, Brazil, *J. Geophys. Res.*, 107, 8083, doi:10.1029/2001JD000523, 2002.
- Koren, V., Schaake, J., Mitchell, K., Duan, Q.-Y., and Chen, F.: A parameterization of snowpack and frozen ground intended for NCEP weather and climate models, *J. Geophys. Res.*, 104, 19569–19585, 1999.
- 5 Kuhn, U., Ganzeveld, L., Thielmann, A., Dindorf, T., Schebeske, G., Welling, M., Sciare, J., Roberts, G., Meixner, F. X., Kesselmeier, J., Lelieveld, J., Kolle, O., Ciccioli, P., Lloyd, J., Trentmann, J., Artaxo, P., and Andreae, M. O.: Impact of Manaus City on the Amazon Green Ocean atmosphere: ozone production, precursor sensitivity and aerosol load, *Atmos. Chem. Phys.*, 10, 9251–9282, doi:10.5194/acp-10-9251-2010, 2010.
- 10 Kummerow, C., Barnes, W., Kozu, T., Shiue, J., and Simpson, J.: The Tropical Rainfall Measuring Mission (TRMM) sensor package, *J. Atmos. Ocean. Tech.*, 15, 809–816, 1998.
- Lelieveld, J., Butler, T. M., Crowley, J. N., Dillon, T. J., Fischer, H., Ganzeveld, L., Harder, H., Lawrence, M. G., Martinez, M., Taraborrelli, D., and Williams, J.: Atmospheric oxidation capacity sustained by a tropical forest, *Nature*, 452, 737–740, 2008.
- 15 Logan, J. A.: Tropospheric ozone: seasonal behavior, trends, and anthropogenic influence, *J. Geophys. Res.*, 90, 10463–10482, 1985.
- Logan, J. A.: An analysis of ozonesonde data for the troposphere: recommendations for testing 3-D models and development of a gridded climatology for tropospheric ozone, *J. Geophys. Res.*, 104, 16115–16149, 1999.
- 20 Longo, K. M., Thompson, A. M., Kirchhoff, V. W. J. H., Remer, L. A., de Freitas, S. R., Dias, M. A. F. S., Artaxo, P., Hart, W., Spinhirne, J. D., and Yamasoe, M. A.: Correlation between smoke and tropospheric ozone concentration in Cuiabá during Smoke, Clouds, and Radiation-Brazil (SCAR-B), *J. Geophys. Res.*, 104, 12113–12129, doi:10.1029/1999JD900044, 1999.
- 25 Longo, K. M., Freitas, S. R., Andreae, M. O., Yokelson, R., Artaxo, P., Biomass burning in Amazonia: emissions, long-range transport of smoke and its regional and remote impacts, in: *Amazonia and Global Change*, edited by: Keller, M., Bustamante, M., Gash, J., and Silva Dias, P., vol. 186, AGU Geoph. Monog. Series, Washington DC, 2009.
- 30 Longo, K. M., Freitas, S. R., Pirre, M., Marécal, V., Rodrigues, L. F., Panetta, J., Alonso, M. F., Rosário, N. E., Moreira, D. S., Gácita, M. S., Arteta, J., Fonseca, R., Stockler, R., Katsurayama, D. M., Fazenda, A., and Bela, M.: The Chemistry CATT-BRAMS model (CATT-BRAMS 4.5): a regional atmospheric model system for integrated air quality and weather

14041

- forecasting and research, *Geosci. Model Dev.*, 6, 1389–1405, doi:10.5194/gmd-6-1389-2013, 2013.
- Martin, S. T., Andreae, M. O., Althausen, D., Artaxo, P., Baars, H., Borrmann, S., Chen, Q., Farmer, D. K., Guenther, A., Gunthe, S. S., Jimenez, J. L., Karl, T., Longo, K., Manzi, A., Müller, T., Pauliquevis, T., Petters, M. D., Prenni, A. J., Pöschl, U., Rizzo, L. V., Schneider, J., Smith, J. N., Swietlicki, E., Tota, J., Wang, J., Wiedensohler, A., and Zorn, S. R.: An overview of the Amazonian Aerosol Characterization Experiment 2008 (AMAZE-08), *Atmos. Chem. Phys.*, 10, 11415–11438, doi:10.5194/acp-10-11415-2010, 2010.
- 5 Mellor, G. L. and Yamada, T.: Development of a turbulence closure model for geophysical fluid problems, *Rev. Geophys. Space Phys.*, 20, 851–875, 1982.
- 10 Reich, P. B. and Amundson, R. G.: Ambient levels of ozone reduce net photosynthesis in tree and crop species, *Science*, 230, 566–570, doi:10.1126/science.230.4725.566, 1985.
- Rinne, H. J. I., Guenther, A. B., Greenberg, J. P., and Harley, P. C.: Isoprene and monoterpene fluxes measured above Amazonian rainforest and their dependence on light and temperature, *Atmos. Environ.*, 36, 2421–2426, doi:10.1016/S1352-2310(01)00523-4, 2002.
- 15 Rosário, N. M. E.: Variability of aerosol optical properties over South America and the impacts of direct radiative effect of aerosols from biomass burning, Ph.D. thesis, Institute of Astronomy, Geophysics and Atmospheric Sciences, University of São Paulo, São Paulo, 2011 (in Portuguese).
- 20 Rosário, N. E., Longo, K. M., Freitas, S. R., Yamasoe, M. A., and Fonseca, R. M.: Modeling the South American regional smoke plume: aerosol optical depth variability and surface shortwave flux perturbation, *Atmos. Chem. Phys.*, 13, 2923–2938, doi:10.5194/acp-13-2923-2013, 2013.
- Rummel, U., Ammann, C., Kirkman, G. A., Moura, M. A. L., Foken, T., Andreae, M. O., and Meixner, F. X.: Seasonal variation of ozone deposition to a tropical rain forest in southwest Amazonia, *Atmos. Chem. Phys.*, 7, 5415–5435, doi:10.5194/acp-7-5415-2007, 2007.
- Sestini, M., Reimer, E., Valeriano, D., Alvalá, R., Mello, E., Chan, C., and Nobre, C.: Mapa de cobertura da terra da Amazônia legal para uso em modelos meteorológicos, *Anais XI Simpósio Brasileiro de Sensoriamento Remoto*, 2901–2906, 2003.
- 30 Sigler, J. M., Fuentes, J. D., Heitz, R. C., Garstang, M., and Fisch, G.: Ozone dynamics and deposition processes at a deforested site in the Amazon Basin, *Ambio*, 31, 21–27, doi:10.1579/0044-7447-31.1.21, 2002.

14042

- Silva, C. M. S., Freitas, S. R., Gielow, R., and Barros, S. S.: Evaluation of high-resolution precipitation estimate over the Amazon Basin, *Atmos. Sci. Lett.*, 10, 273–278, doi:10.1002/asl.242, 2009.
- Silva, C. M. S., Freitas, S. R., and Gielow, R.: Numerical simulation of the diurnal cycle of rainfall in SW Amazon Basin during the 1999 rainy season: the role of convective trigger function, *Theor. Appl. Climatol.*, 109, 473–483, doi:10.1007/s00704-011-0571-0, 2012.
- Stockwell, D. Z., Giannakopoulos, C., Plantevin, P.-H., Carver, G. D., Chipperfield, M. P., Law, K. S., Pyle, J. A., Shallcross, D. E., and Wang, K.-Y.: Modeling NO_x from lightning and its impact on global chemical fields, *Atmos. Environ.*, 33, 4477–4493, doi:10.1016/S1352-2310(99)00190-9, 1999.
- Stockwell, W. R., Kirchner, F., and Kuhn, M.: A new mechanism for regional chemistry modeling, *J. Geophys. Res.*, 102, 25847–25879, doi:10.1029/97JD00849, 1997.
- Thompson, A. M., Pickering, K. E., McNamara, D. P., Schoeberl, M. R., Hudson, R. D., Kim, J. H., Browell, E. V., Kirchhoff, V. W. J. H., and Nganga, D.: Where did tropospheric ozone over southern Africa and the tropical Atlantic come from in October 1992? Insights from TOMS, GTE TRACE A, and SAFARI 1992, *J. Geophys. Res.*, 101, 24251–24278, doi:10.1029/96JD01463, 1996.
- Thompson, A. M., Witte, J. C., McPeters, R. D., Oltmans, S. J., Schmidlin, F. J., Logan, J. A., Fujiwara, M., Kirchhoff, V. W. J. H., Posny, F., Coetzee, G. J. R., Hoegger, B., Kawakami, S., Ogawa, T., Johnson, B. J., Vömel, H., and Labo, G.: Southern Hemisphere Additional Ozonesondes (SHADOZ) 1998–2000 tropical ozone climatology 1. Comparison with Total Ozone Mapping Spectrometer (TOMS) and ground-based measurements, *J. Geophys. Res.*, 108, 8238, doi:10.1029/2001JD000967, 2003a.
- Thompson, A. M., Witte, J. C., Oltmans, S. J., Schmidlin, F. J., Logan, J. A., Fujiwara, M., Kirchhoff, V. W. J. H., Posny, F., Coetzee, G. J. R., Hoegger, B., Kawakami, S., Ogawa, T., Fortuin, J. P. F., and Kelder, H. M.: Southern Hemisphere Additional Ozonesondes (SHADOZ) 1998–2000 tropical ozone climatology 2. Tropospheric variability and the zonal wave-one, *J. Geophys. Res.*, 108, 8241, doi:10.1029/2002JD002241, 2003b.
- Thompson, A. M., Witte, J. C., Smit, H. G. J., Oltmans, S. J., Johnson, B. J., Kirchhoff, V. W. J. H., and Schmidlin, F. J.: Southern Hemisphere Additional Ozonesondes (SHADOZ) 1998–2004 tropical ozone climatology: 3. Instrumentation, station-to-station variability, and evaluation with simulated flight profiles, *J. Geophys. Res.*, 112, D03304, doi:10.1029/2005JD007042, 2007.

14043

- Toon, O. B., Starr, D. O., Jensen, E. J., Newman, P. A., Platnick, S., Schoeberl, M. R., Wennberg, P. O., Wofsy, S. C., Kurylo, M. J., Maring, H., Jucks, K. W., Craig, M. S., Vasques, M. F., Pfister, L., Rosenlof, K. H., Selkirk, H. B., Colarco, P. R., Kawa, S. R., Mace, G. G., Minnis, P., and Pickering, K. E.: Planning, implementation, and first results of the Tropical Composition, Cloud and Climate Coupling Experiment (TC4), *J. Geophys. Res.*, 115, D00J04, doi:10.1029/2009JD013073, 2010.
- Torres, A. L. and Buchan, H.: Tropospheric nitric oxide measurements over the Amazon Basin, *J. Geophys. Res.*, 93, 1396–1406, doi:10.1029/JD093iD02p01396, 1988.
- Walko, R. L., Band, L. E., Baron, J., Kittel, T. G. F., Lammers, R., Lee, T. J., Ojima, D., Pielke, R. A., Taylor, C., Tague, C., Tremback, C. J., and Vidale, P. L.: Coupled atmosphere-biophysics hydrology models for environmental modeling, *J. Appl. Meteor.*, 39, 931–944, doi:10.1175/1520-0450(2000)039<0931:CABHMF>2.0.CO;2, 2000.
- Wesley, M. L.: Parameterization of surface resistance to gaseous dry deposition in regional numerical models, *Atmos. Environ.*, 16, 1293–1304, 1989.
- Zhang, L., Jacob, D. J., Liu, X., Logan, J. A., Chance, K., Eldering, A., and Bojkov, B. R.: Intercomparison methods for satellite measurements of atmospheric composition: application to tropospheric ozone from TES and OMI, *Atmos. Chem. Phys.*, 10, 4725–4739, doi:10.5194/acp-10-4725-2010, 2010.
- Zhou, J., Swietlicki, E., Hansson, H. C., and Artaxo, P.: Submicrometer aerosol particle size distribution and hygroscopic growth measured in the Amazon rain forest during the wet-to-dry transition season, *J. Geophys. Res.*, 107, 8055, doi:10.1029/2000JD000203, 2002.
- Ziemke, J. R., Chandra, S., Duncan, B. N., Froidevaux, L., Bhartia, P. K., Levelt, P. F., and Waters, J. W.: Tropospheric ozone determined from Aura OMI and MLS: Evaluation of measurements and comparison with the Global Modeling Initiative's Chemical Transport Model, *J. Geophys. Res.*, 111, D19303, doi:10.1029/2006JD007089, 2006.
- Ziemke, J. R., Joiner, J., Chandra, S., Bhartia, P. K., Vasilkov, A., Haffner, D. P., Yang, K., Schoeberl, M. R., Froidevaux, L., and Levelt, P. F.: Ozone mixing ratios inside tropical deep convective clouds from OMI satellite measurements, *Atmos. Chem. Phys.*, 9, 573–583, doi:10.5194/acp-9-573-2009, 2009.

14044

Table 1. CCATT-BRAMS and WRF-Chem physics and chemistry options for the BARCA simulations.

	CCATT-BRAMS	WRF-Chem
Short/longwave radiation	Based on CARMA	RRTMG
Cloud microphysics	Single moment bulk	WSM-5
Deep/shallow convection	Grell and Dévényi (GD)	Grell 3-D
Trace gas chemistry	RACM	RACM
Photolysis	F-TUV	F-TUV
Aerosol scheme	Smoke aerosol	GOCART
Wet deposition	convective and grid scales	convective scale only

14045

Table 2. Monthly mean precipitation (mm h^{-1}) for TRMM 3B43, CCATT-BRAMS and WRF-Chem models for three regions: the Amazon (15°S – 10°N , 50 – 80°W), northeast Brazil (15°S – 0°N , 35 – 50°W), and southeast South America (15 – 35°S , 35 – 65°W).

Region	Nov 2008			May 2009		
	TRMM 3B43	CCATT-BRAMS	WRF-Chem	TRMM 3B43	CCATT-BRAMS	WRF-Chem
Amazon	0.24	0.22	0.51	0.20	0.15	0.40
northeast	0.12	0.07	0.08	0.37	0.23	0.49
southeast	0.19	0.11	0.24	0.10	0.06	0.07

14046

Table 3. Values of RMSE and bias for CCATT-BRAMS and WRF-Chem simulations for 26 METAR and 52 SYNOP stations in the Amazon Basin for BARCA A (October–November 2008) and BARCA B (April–May 2009).

		Oct–Nov 2008			May–Apr 2009		
		Obs.	CCATT-BRAMS	WRF-Chem	Obs.	CCATT-BRAMS	WRF-Chem
T (K)	Mean Obs.	295.97			293.89		
	RMSE		2.30	2.81		1.70	2.44
	Bias		1.04	–2.42		–0.06	–2.28
T_d (K)	Mean Obs.	289.26			288.49		
	RMSE		2.68	1.72		1.76	1.67
	Bias		–1.92	–0.81		–0.99	–0.83
Wind Spd. (m s^{-1})	Mean Obs.	3.00			2.59		
	RMSE		1.41	1.33		1.15	1.00
	Bias		–0.60	0.16		–0.51	0.07
Sfc. Press. (hPa)	Mean Obs.	1013.17			1016.09		
	RMSE		2.16	1.43		1.09	1.34
	Bias		–2.01	–1.02		–0.79	–1.17
Precip. TRMM (mm h^{-1})	Mean Obs.	0.49			0.62		
	RMSE		2.42	4.50		3.03	7.12
	Bias		0.28	3.47		0.25	5.84

14047

Table 4. Average O_3 dry deposition flux ($\text{nmol m}^{-2} \text{s}^{-1}$) and daytime (11:00–21:00 UTC) median deposition velocity (cm s^{-1}) in the dry and wet seasons (Rummel et al., 2007), and WRF-Chem and CCATT-BRAMS simulations from November 2008 (dry-to-wet transition) and May 2009 (wet-to-dry transition) for Reserva Biológica Jarú (RBJ), Fazenda Nossa Senhora (RNS) and Reserva Ducke (RD).

Site		Dry Season			Wet Season		
		Observed	CCATT-BRAMS	WRF-Chem	Observed	CCATT-BRAMS	WRF-Chem
RBJ (forest)	Flux	–5.69	–2.43	–3.25	–2.93	–1.59	–2.39
	v_d	0.6	0.3	0.5	1.2	0.4	0.8
FNS (pasture)	Flux	–4.68	–3.06	–2.49	–2.04	–2.07	–2.04
	v_d	0.6	0.4	0.4	0.7	0.4	0.7
RD (forest)	Flux				–1.82	–1.63	–2.68
	v_d				1.6	0.4	0.6

14048

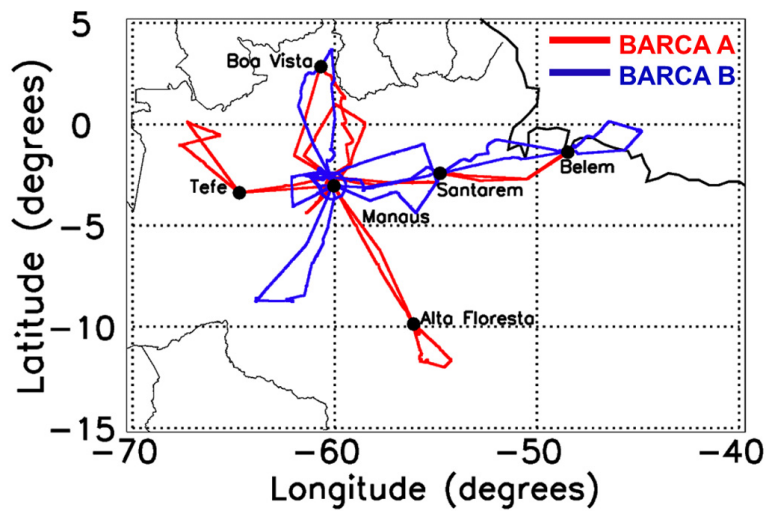


Figure 1. Flight tracks during BARCA.

14049

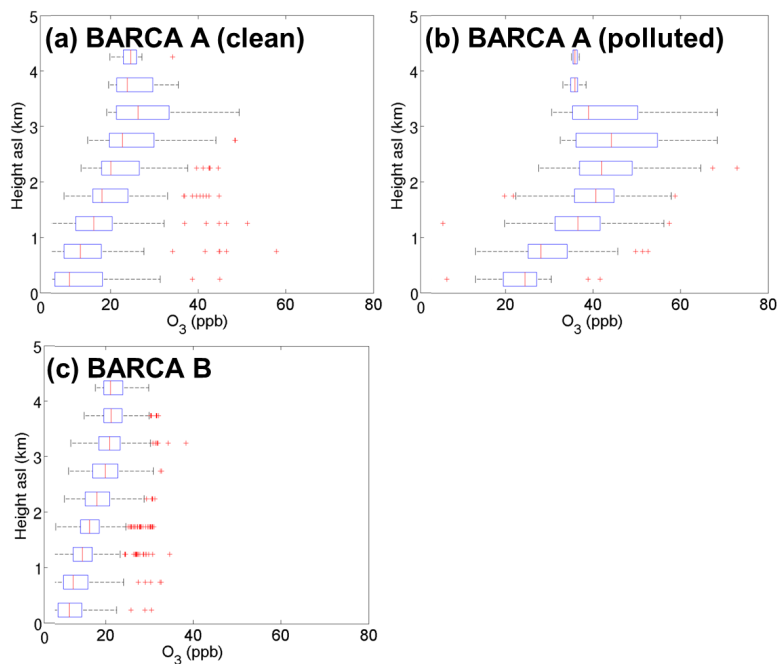


Figure 2. O₃ observations during (a) BARCA A, clean conditions (west, north and around Manaus regions), (b) BARCA A, polluted conditions (east and south regions) and (c) BARCA B. The central mark is the median, the edges of the box are the 25th and 75th percentiles, the whiskers extend to the most extreme data points not considered outliers (as defined by Matlab) and outliers are plotted individually as red pluses.

14050

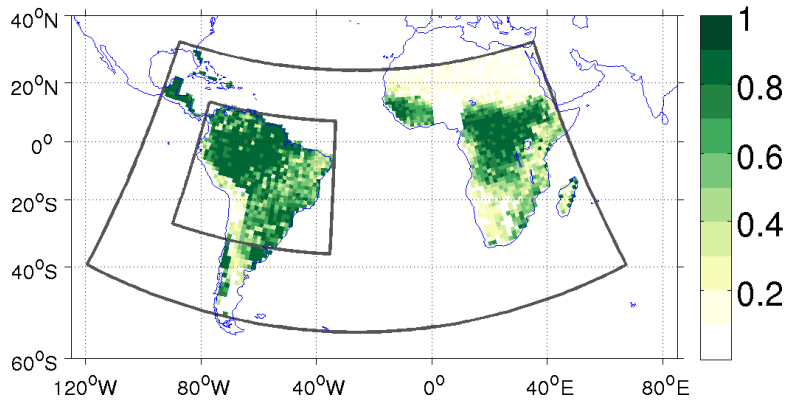


Figure 3. Land surface albedo (fraction) and locations of the coarse (140 km resolution) and nested (35 km resolution) domains for WRF-Chem simulations.

14051

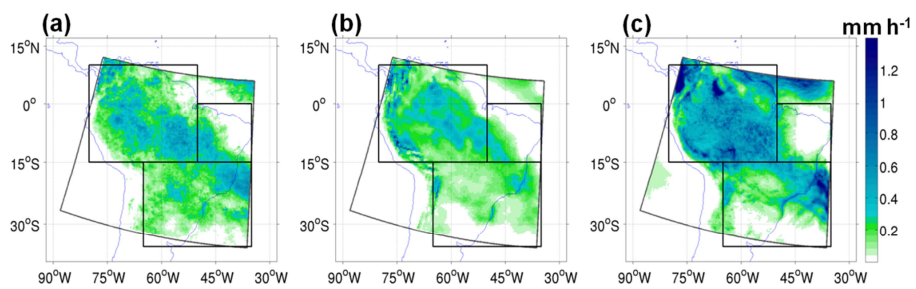


Figure 4. Monthly mean precipitation (mm h^{-1}) for November 2008 on the 35 km resolution domain (dark gray line) from (a) TRMM 3B43, (b) CCATT-BRAMS and (c) WRF-Chem. The subregions for precipitation comparison are indicated by black lines.

14052

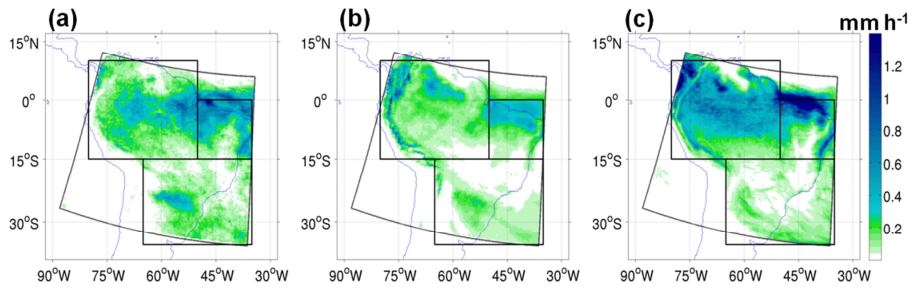


Figure 5. Same as Fig. 4, but for May 2009.

14053

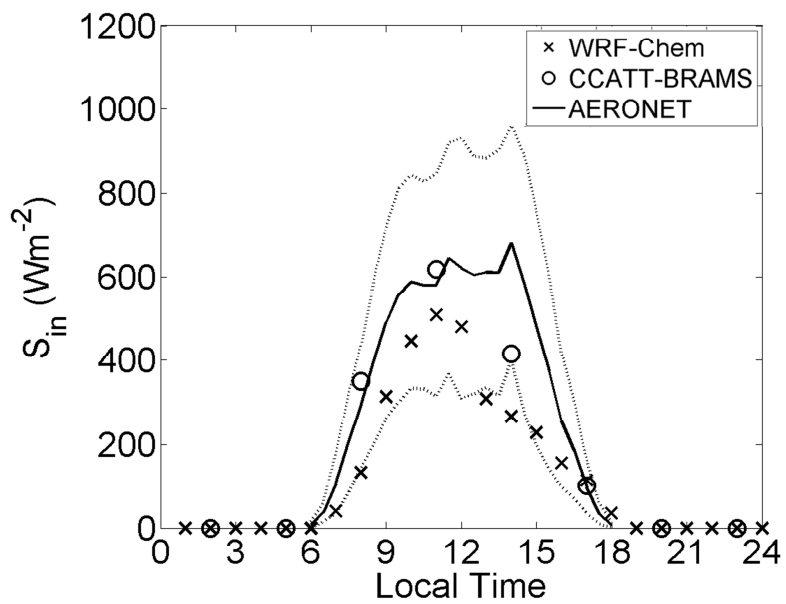


Figure 6. Mean daily cycle of surface incident shortwave radiation from the Manaus AERONET site (solid line, dotted line denotes one standard deviation), WRF-Chem (crosses) and CCATT-BRAMS (circles) for the BARCA A period (October–November 2008).

14054

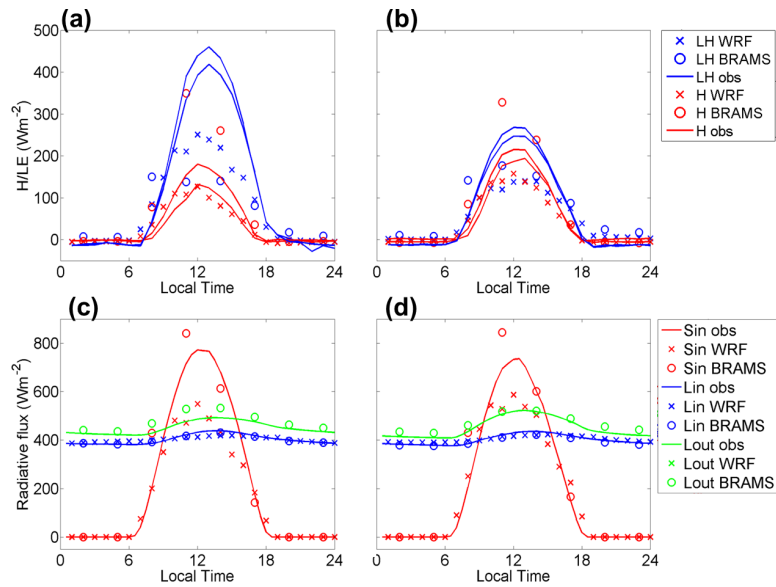


Figure 7. Mean daily cycles of surface (a) latent (LE) and sensible (H) heat and (c) incident shortwave (S_{in}) and incoming (L_{in}) and outgoing (L_{out}) longwave radiation fluxes for a forest site and (b) heat and (d) radiation fluxes for a pasture site, comparing observations (solid lines) from von Randow et al. (2004) for the dry-to-wet transition season (July–September 1999–2000) and from WRF-Chem (crosses) and CCATT-BRAMS (circles) for the BARCA A period (October–November 2008).

14055

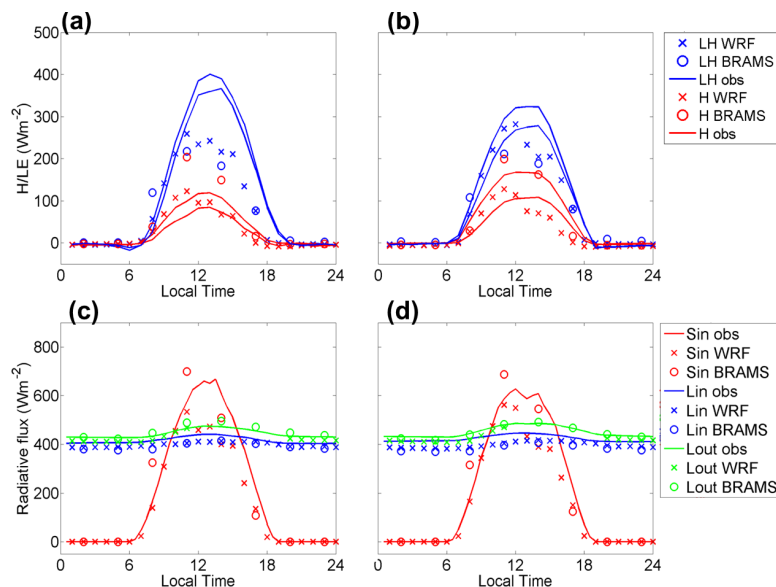


Figure 8. Mean daily cycles of surface (a) latent (LE) and sensible (H) heat and (c) incident shortwave (S_{in}) and incoming (L_{in}) and outgoing (L_{out}) longwave radiation fluxes for a forest site and (b) heat and (d) radiation fluxes for a pasture site, comparing observations (solid lines) from von Randow et al. (2004) for the wet-to-dry transition season (February–March 1999, January–March 2000) and from WRF-Chem (crosses) and CCATT-BRAMS (circles) for the BARCA B period (April–May 2009).

14056

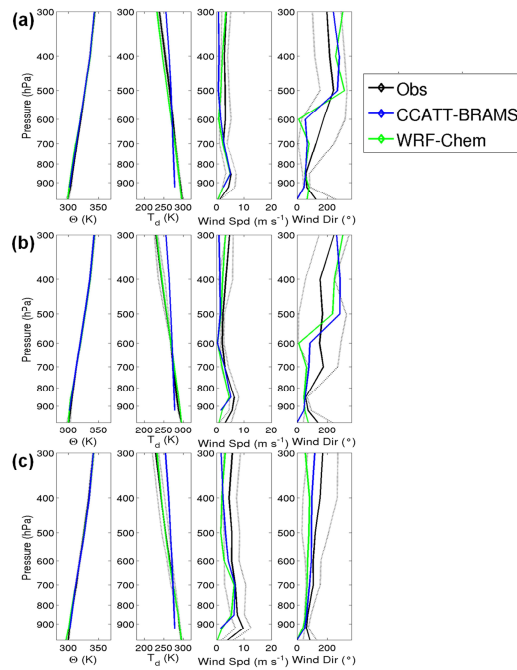


Figure 9. Mean vertical profiles at Manaus from radiosoundings (black, gray line denotes one standard deviation), CCATT-BRAMS (blue) and WRF-Chem (green) for October–November 2008 at (a) 0, (b) 12 and (c) 18Z.

14057

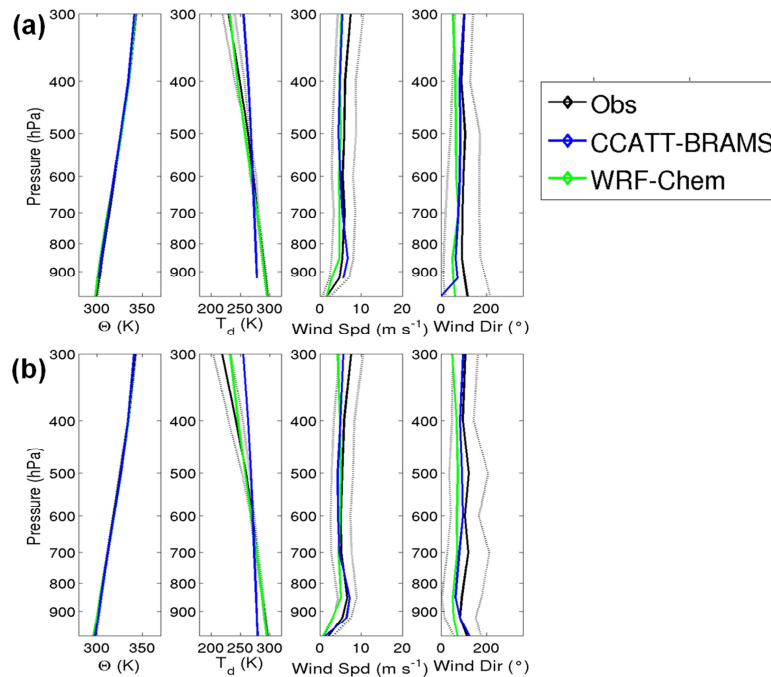


Figure 10. Mean vertical profiles at Manaus from radiosoundings (black, gray line denotes one standard deviation), CCATT-BRAMS (blue) and WRF-Chem (green) for April–May 2009 at (a) 0 and (b) 12Z.

14058

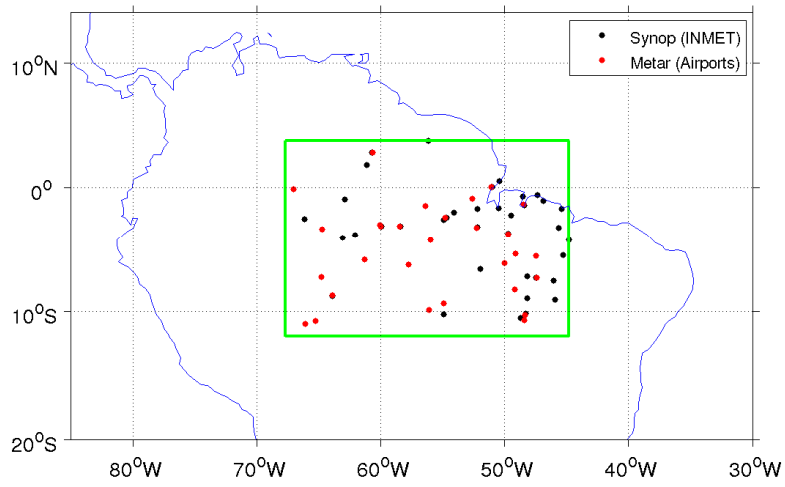


Figure 11. Locations of surface meteorological stations for model evaluation.

14059

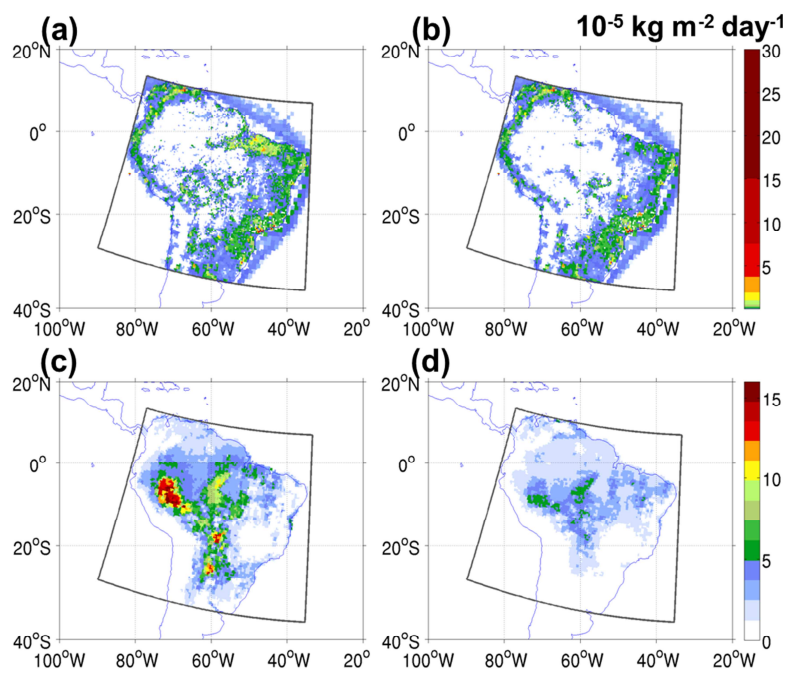


Figure 12. Mean emission rates ($10^{-5} \text{ kg m}^{-2} \text{ d}^{-1}$) from PREP-CHEM-SRC for the 35 km domain (dark gray outline) for NO_x for (a) BARCA A (November 2008) and (b) BARCA B (May 2009) and isoprene for (c) BARCA A and (d) BARCA B periods.

14060

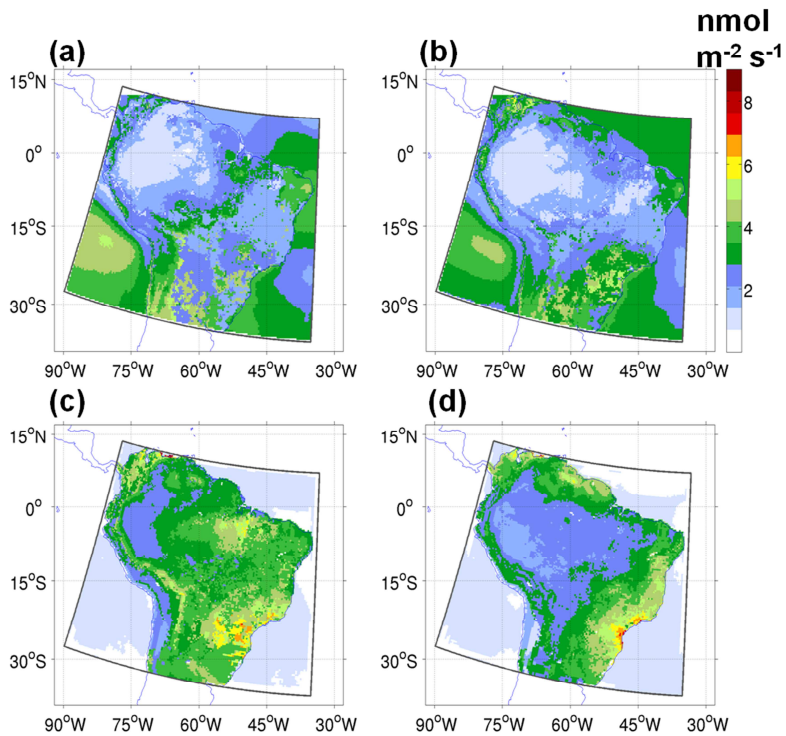


Figure 13. Average O₃ dry deposition flux ($\text{nmol m}^{-2} \text{s}^{-1}$) as simulated on the 35 km resolution domain (dark gray outline) by the CCATT-BRAMS model for (a) November 2008 and (b) May 2009 and by the WRF-Chem model for (c) November 2008 and (d) May 2009.

14061

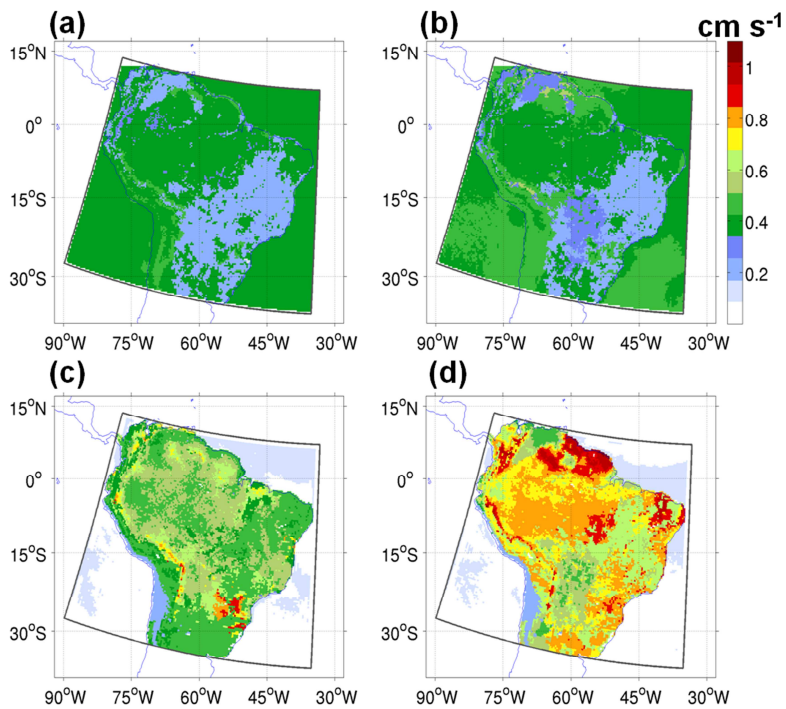


Figure 14. Same as Fig. 13, but daytime (11:00–21:00 UTC) median deposition velocity (cm s^{-1}).

14062

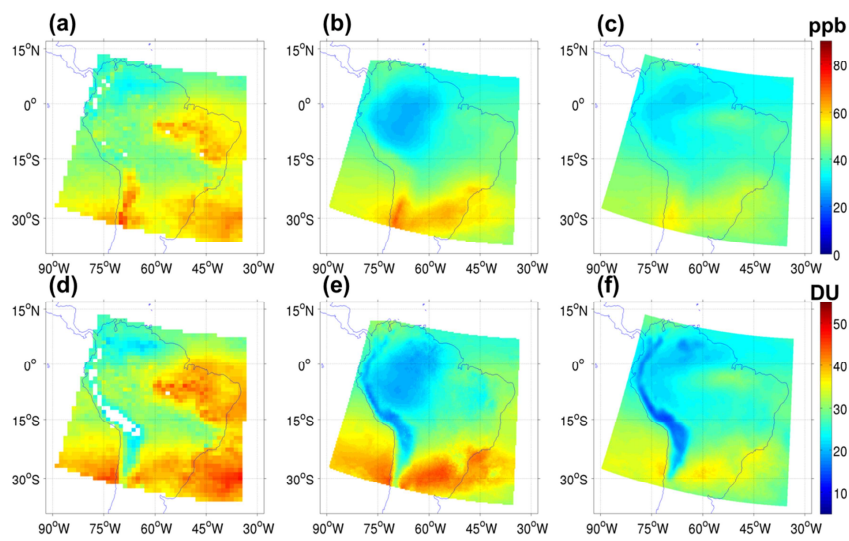


Figure 15. Mean tropospheric O₃ (ppb) on the 35 km domain from (a) OMI/MLS, (b) CCATT-BRAMS and (c) WRF-Chem and total tropospheric column O₃ (Dobson units) from (d) OMI/MLS, (e) CCATT-BRAMS and (f) WRF-Chem for November 2008.

14063

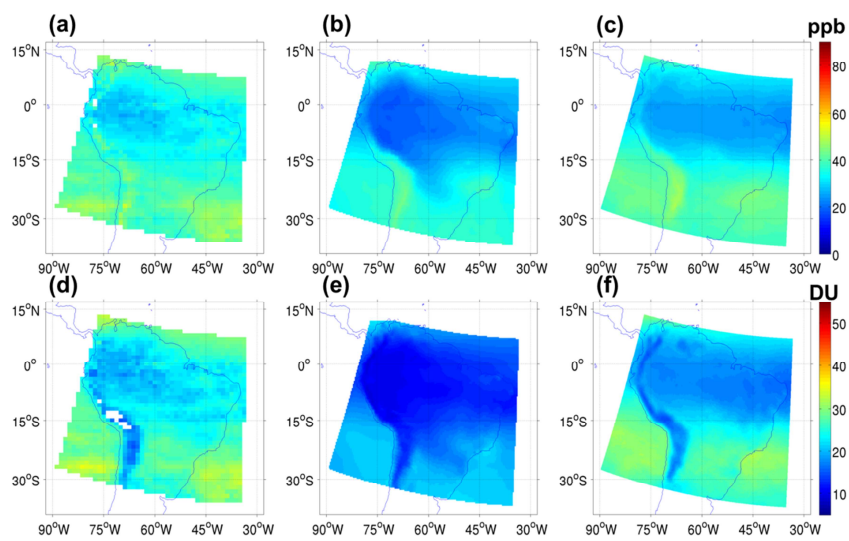


Figure 16. Same as Fig. 15, but for May 2009.

14064

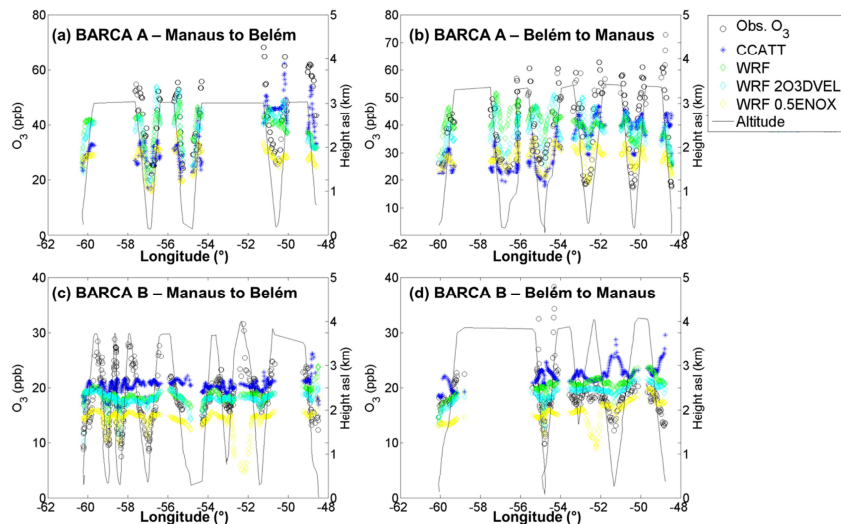


Figure 17. O_3 as observed (black circles) and simulated with CCATT-BRAMS (blue stars) and WRF-Chem (base case – green diamonds, 2DEPVEL – cyan circles and 0.5ENOX – yellow squares) from BARCA flights **(a)** from Manaus to Belém on November 18, 2008, **(b)** Belém to Manaus on November 19, 2008, **(c)** Manaus to Belém on 21 May 2009 and **(d)** Belém to Manaus on November 23, 2009.

14065

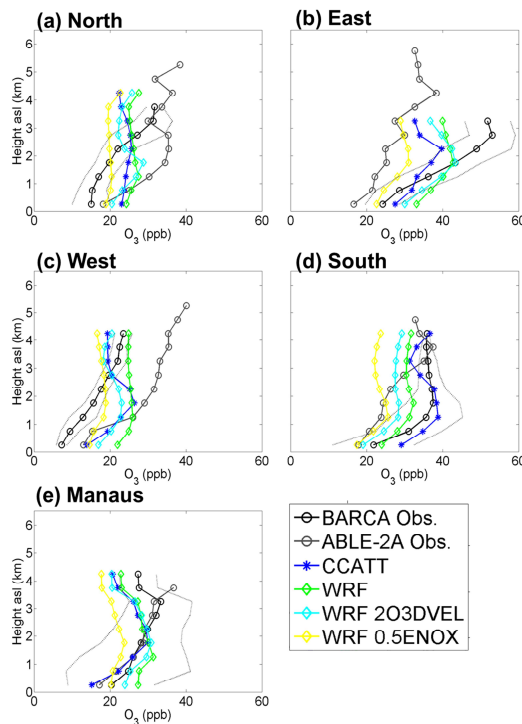


Figure 18. Mean vertical O_3 profiles for BARCA A flights for observations (black, gray line denotes one standard deviation), CCATT-BRAMS (blue) and WRF-Chem (base case – green, 2DEPVEL – cyan and 0.5ENOX – yellow) simulations by region: **(a)** north, **(b)** east, **(c)** west, **(d)** south, and **(e)** around Manaus. ABLÉ-2A observations (gray) from the same regions are included for comparison.

14066

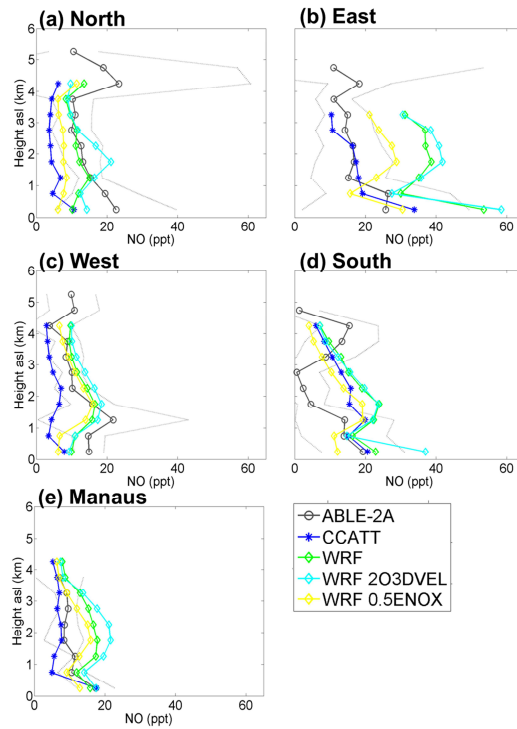


Figure 19. Mean vertical NO profiles corresponding to BARCA A flights for CCATT-BRAMS (blue) and WRF-Chem (base case – green, 2DEPVEL – cyan and 0.5ENox – yellow) simulations by region: **(a)** north, **(b)** east, **(c)** west, **(d)** south, and **(e)** around Manaus. ABL-2A observations (gray) from the same regions are included for comparison.

14067

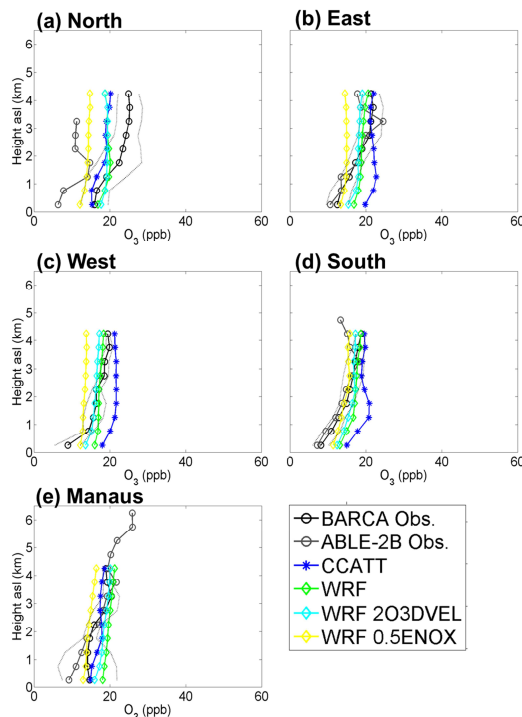


Figure 20. Mean vertical O₃ profiles for BARCA B flights for observations (black, gray line denotes one standard deviation), CCATT-BRAMS (blue) and WRF-Chem (base case – green, 2DEPVEL – cyan and 0.5ENox – yellow) simulations by region **(a)** north, **(b)** east, **(c)** west, **(d)** south, and **(e)** around Manaus. ABL-2A observations (gray) from the same regions are included for comparison.

14068

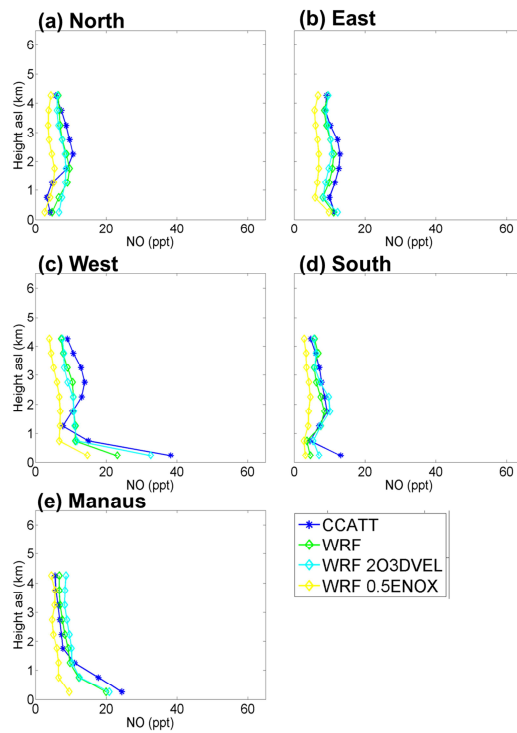


Figure 21. Mean vertical NO profiles corresponding to BARCA B flights for CCATT-BRAMS (blue) and WRF-Chem (base case – green, 2DEPVEL – cyan and 0.5ENOX – yellow) simulations by region: **(a)** north, **(b)** east, **(c)** west, **(d)** south, and **(e)** around Manaus.

14069

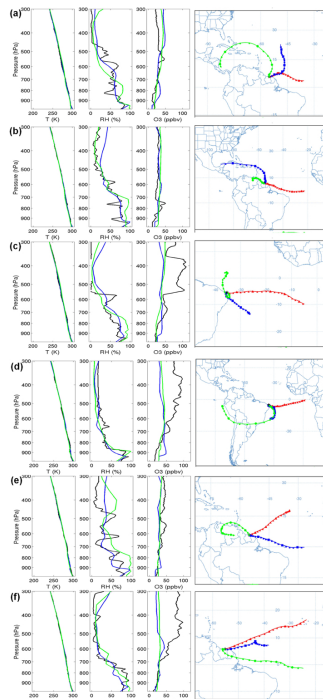


Figure 22. Vertical profiles of potential temperature, relative humidity, and O_3 from SHADOZ soundings (black), CCATT-BRAMS (blue) and WRF-Chem (green) and HYSPLIT back trajectories at 1500 m (~ 850 hPa, red), 6000 m (~ 470 hPa, blue) and 9000 m (~ 310 hPa, green) for: Paramaribo on **(a)** November 6 and **(b)** November 25, 2008, Natal on **(c)** November 7 and **(d)** November 19, 2008 and Paramaribo on **(e)** 4 May and **(f)** 11 May 2009.

14070